UNIVERSITY OF ILLINOIS
URBANA

AERONOMY REPORT NO. 21

POSITIVE ION COLLECTION BY A SPHERICAL PROBE IN A COLLISION-DOMINATED PLASMA

by
R. J. Cicerone
S. A. Bowhill

June 1, 1967

Supported by
National Aeronautics and
Space Administration
Grant NsG-511

Aeronomy Laboratory
Department of Electrical Engineering
University of Illinois
Urbana, Illinois

AERONOMY REPORT NO. 21

POSITIVE ION COLLECTION BY A SPHERICAL PROBE IN A COLLISION-DOMINATED PLASMA

by

R. J. Cicerone
S. A. Bowhill

June 1, 1967

Supported by
National Aeronautics and Space Administration
Grant NsG-511

Aeronomy Laboratory
Department of Electrical Engineering
University of Illinois
Urbana, Illinois

ABSTRACT

The theory of operation of electrostatic probes in a slightly ionized, collision-dominated gas, such as the D-region of the ionosphere, is poorly understood. This report studies the collection of positive ions by a highly negative spherical probe in such a plasma for ratios of probe radius to Debye length of the order of unity.

The theory is reviewed and the governing equations are developed. Due to the nonlinearity of the equations, a numerical method was necessary to solve the equations exactly. This method is explained in detail. The results are compared to those of Su and Lam (1963) and to the results of a zero space-charge theory. It is concluded that space charge may not be neglected.

TABLE OF CONTENTS

TABLE OF CONTENTS (continued)

LIST OF TABLES

LIST OF ILLUSTRATIONS

1. RELEVANT PROPERTIES OF THE LOWER IONOSPHERE

1.1 Qualitative Description of the Lower Ionosphere

The ionosphere is a weakly ionized gas which completely envelopes the earth. It extends from 50 km in altitude to perhaps 1000 km and is permeated by the earth's magnetic field. The lower ionosphere, as designated by Whitten and Poppoff (1965), is the altitude region between 50 and 150 km. The principal source of ionizing electromagnetic radiation is the sun but galactic cosmic rays are also important. With increasing altitude the degree of ionization tends to increase, while the absolute concentration of charged particles exhibits a layered structure associated with different photoionization and recombination processes. That such layers are likely to form in the ionosphere can be seen from elementary considerations and is discussed clearly by Belrose (1965). This structure provides a convenient, but by no means unique method of classifying the various altitude regions. According to the physical processes under study other classification schemes may be chosen, such as those based on neutral gas temperature profiles, chemical composition, or ionization dynamics.

Ground-based radio techniques provide a convenient method of studying the ionization above 85 km in altitude. A well-defined layer of ionization is formed during normal daytime conditions in the altitude region between 90 and 150 km and is known as the E-region. The F-region extends upward from the top of the E-region. No convention has been adopted regarding the upper limit of the F-region. The earliest studies of the ionosphere revealed directly the existence of the E- and F-regions but they also gave indirect evidence for an ionized layer below 90 km in

altitude (Appleton and Ratcliffe, 1930). This altitude regime has come to be called the D-region. Some evidence for the existence of another even lower layer (the C-region) has been obtained from the study of low frequency radio wave propagation (Krasnushkin and Kolesnikov, 1962).

1.2 Description of the D- and E-Regions in Terms of Plasma Parameters

A very small fraction of the gas molecules in the D-region are ionized. Measurements of the concentrations of the charged particles there are difficult and data is therefore scarce. Profiles of D-region electron densities may be obtained by ground-based (partial reflection) experiments; see e.g. (Belrose and Burke, 1964). Figure 1.1 shows the number densities of positive ions, negative ions, and electrons plotted versus altitude as obtained by Sagalyn and Smiddy (1964) in a daytime rocket experiment. These number densities of 10^3 or 10^4 cm^{-3} may be compared with the neutral gas number density profile shown in Figure 1.2 which is due to Champion and Minzer (1963).

At night the electrons recombine by attachment to neutral molecules, forming negative ions. In visible light these negative ions are unstable (Belrose, 1965). Estimates of the ratio, λ, of negative ion concentration to the electron concentration range from 7.5 at 60 km to 10^3 at 90 km in the daytime (Nicolet and Aikin, 1960). Nighttime measurements by Sagalyn (1965) show that λ is greater than unity to altitudes above 90 km, and this ratio should increase approximately exponentially with decreasing altitude since the electron-neutral collision frequency is proportional to the neutral gas number density.

The electron temperature in the D-region is virtually identical to the neutral gas temperature (Salah and Bowhill, 1966) and the same is generally regarded as true for the positive and negative ions since they

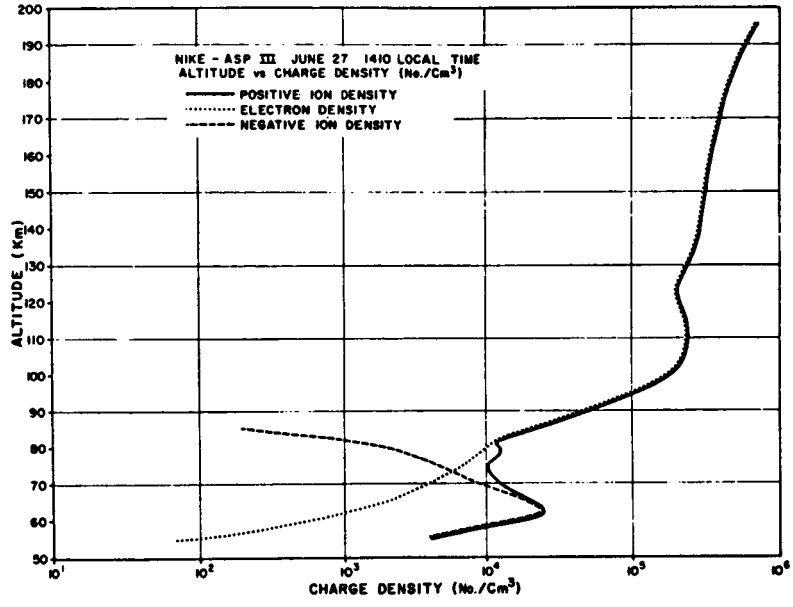

Figure 1.1 Number densities of positive ions, negative ions, and electrons versus altitude (after Sagalyn and Smiddy, 1964).

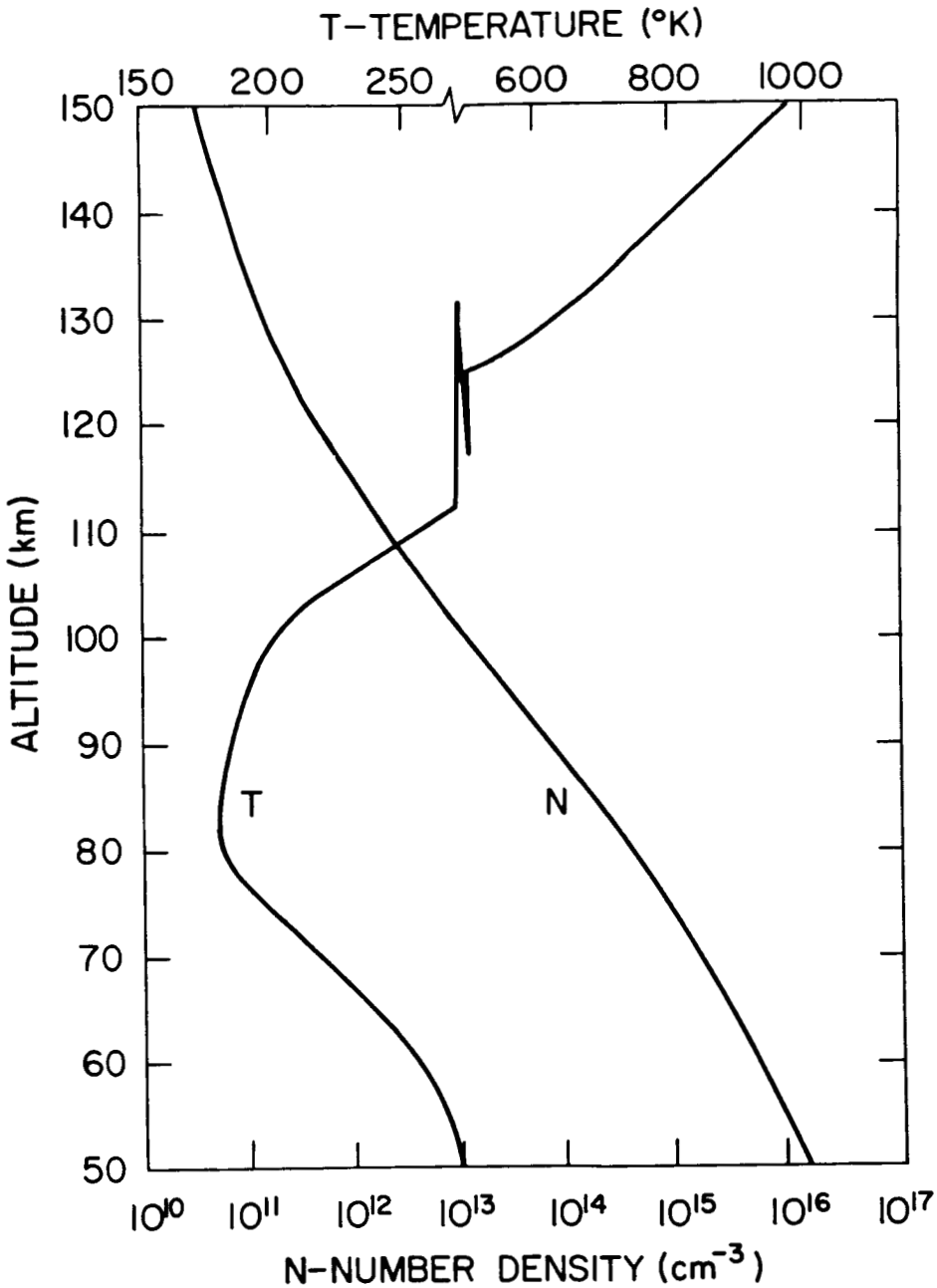

Figure 1.2 Neutral gas number density and temperature versus altitude (after Champion and Minzer, 1963).

are in even better thermal contact with the neutrals than the electrons. The temperature profile shown in Figure 1.2 and the positive ion densities shown in Figure 1.1 lead to a Debye length for positive ions which varies roughly between 0.4 cm and 4.0 cm in the D-region. The Debye length, λ_D, of a charged particle species is given approximately by

$$\lambda_D = 6.91 \ (T/N_o)^{1/2} \tag{1.1}$$

where T is the temperature of the species in degrees Kelvin, and N_o is the number density of the same species in cm^{-3}.

Since such a small fraction of the gas molecules in the D-region is ionized, collisions of charged particles with neutral molecules are much more frequent than collisions with other charged particles. In illustration, the mean free path for electron-ion collisions, ℓ_{e-i}, lies between 10^5 cm and 10^7 cm, computed from the relation from Boyd (1966):

$$\ell_{e-i} = \frac{1.6 \times 10^5 \ T_e^2}{n_e \ [0.8 + \ln \ (T_e^3/ne)]} \tag{1.2}$$

The ion-neutral mean free path, ℓ, assuming N_2^+ ions in N_2 gas, cross-section data from McDaniel (1964), and the neutral gas density profile of Figure 1.2, is subject to:

$$10^{-2} \text{ cm} < \ell < 1.0 \text{ cm}$$

in the D-region. The neutral-neutral mean free path, ℓ_{nn}, given approximately by

$$\ell_{nn} = 4 \times 10^{14}/n_n \quad \text{cm} \tag{1.3}$$

where n_n is the neutral gas number density in cm^{-3} ranges between 4×10^{-2} cm and 4.0 cm, from the data of Figure 1.2.

Measurements of charged-particle parameters in the E-region are much easier than in the D-region. Electron density versus altitude profiles can be obtained with a good accuracy by a variety of techniques. An electron density profile determined from an ionosonde record by Bowhill and Schmerling (1961) is shown in Figure 1.3. Other experimental investigations (Sagalyn and Smiddy, 1964) have shown that, at least in the daytime, there are no negative ions at altitudes as high as the E-region. Thus, charge neutrality requires the positive ion density to be the same as the electron density. This condition is apparent in Figure 1.1.

The E-region electron temperature generally exceeds the neutral gas temperature. Spencer et al. (1965) and Smith et al. (1965) have reported E-region electron temperature measurements by rocket-borne Langmuir probes. Their results show that the difference between the electron temperature and the neutral gas temperature can be as much as twice the neutral gas temperature, according to the phase of the sunspot cycle, season, time of day, and other factors.

E-region values of the electron-ion mean free path, given by Equation (1.2), range between 4×10^4 cm and 5×10^5 cm. The neutral-neutral mean free path from Equation (1.3) varies between 40 cm and 8×10^3 cm, while the positive ion Debye length is approximately 0.3 cm throughout the E-region.

The values of charged-particle parameters just cited are the pertinent lengths for a theory of electrostatic probes in the lower ionosphere which neglects the earth's magnetic field. Table 1.1, taken

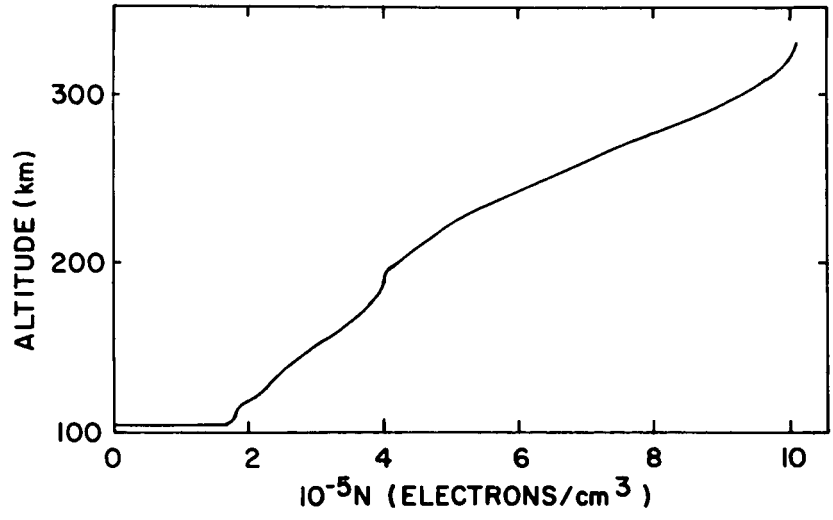

Figure 1.3 An electron density profile determined from an ionosonde record (after Bowhill and Schmerling, 1961).

from a chart of Boyd (1965), compares the ion-neutral mean free path and the ionic Debye length with the linear dimension, r_p, of a practical present-day rocket-borne probe for the various altitudes of the lower ionosphere.

Height Range	Conditions
above 85 kilometers	$\ell > \lambda_D > r_p$
	$\ell > r_p > \lambda_D$
	$r_p > \ell > \lambda_D$
below 85 kilometers	$\lambda_D > \ell > r_p$
	$r_p > \lambda_D > \ell$
	$\lambda_D > r_p > \ell$

Table 1.1 Relations between mean free path, Debye length, and a practical probe radius in the lower ionosphere.

The physical theories applicable to the various conditions listed in Table 1.1 will be discussed in Chapter 2.

2. THE USE OF ELECTROSTATIC PROBES IN THE LOWER IONOSPHERE

2.1 Introduction

One of the fundamental techniques for measuring the properties of plasmas is the use of electrostatic probes. This method of investigation was highly developed by Langmuir and his colleagues as early as 1924. Basically, an electrostatic probe is a small metallic electrode inserted into a plasma. The probe is attached to a DC power supply capable of biasing it at various voltages positive or negative with respect to the plasma, and the current collected by the probe then provides information about the conditions in the plasma, such as the concentrations and energy distributions of the charged particles. Under a wide range of conditions, the disturbance caused by the presence of the probe is localized and the quantity being measured is perturbed only to a very small degree. In some situations, however, such as in the presence of a strong magnetic field, the disturbance is not localized and the current drawn by the probe usually carries considerably less information. Also, since a probe appears as a boundary to a plasma the theory of probes is very complicated; near the boundary the equations governing the motion of the plasma change in character.

In spite of the many difficulties, both experimental and theoretical, arising from the use of probes in plasmas, the method is of fundamental importance since it has one distinct advantage over all other diagnostic techniques: it can make local measurements. Almost all other techniques, such as spectroscopy and radio wave propagation, give information averaged over a large volume of plasma. Even in the cases where the probe current cannot be clearly interpreted in terms of the exact values of

the plasma parameters near the probe, one can still deduce relative values and their fluctuations.

2.2 Types of DC Probes Used in the Lower Ionosphere

2.2.1 Langmuir Probes

Before examining the theory of Langmuir probes, it should be noted that implicit in any probe theory is the notion of a sheath. In the region adjacent to a probe (or any boundary) in a plasma, charge neutrality need not be and usually is not satisfied as it is in the undisturbed plasma away from the probe. Electric fields may therefore exist in this layer and a potential difference appears between the probe surface and the ambient plasma. This layer over which a potential difference exists is the sheath. Ascribing a definite thickness to the sheath is an approximation which has led to useful theoretical results and which serves as a criterion for the applicability of the classical Langmuir probe theory. This criterion will be discussed later. While the thickness of the sheath surrounding a probe varies with probe potential (Bettinger and Walker, 1964) it is convenient to express the scale of thickness in terms of the plasma parameters by the Debye shielding length, λ_D, given by Equation (1.1).

First we will examine the current-voltage characteristic of a Langmuir probe. In Figure 2.1 the negative, or electron current to a Langmuir probe in a plasma consisting of positive ions, electrons and neutrals is plotted versus the probe potential with respect to an arbitrary reference point. Such a plot may be obtained in various ways: continuously in a steady-state plasma, or point by point in a pulsed discharge, the probe bias being changed from pulse to pulse. At the

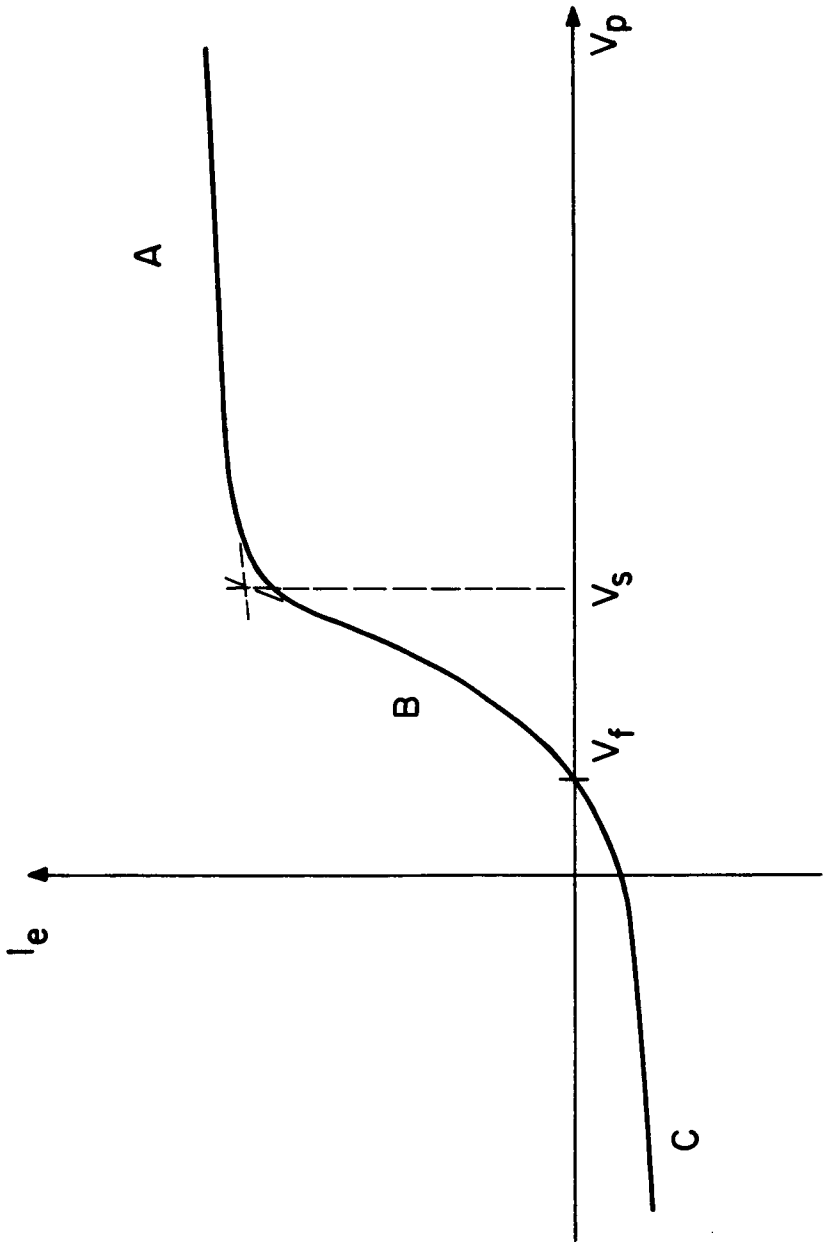

Figure 2.1 Current-voltage characteristics of a Langmuir probe.

line $V_p = V_s$ the probe is at the plasma, or space, potential and there are no electric fields present The current collected by the probe is entirely due to the thermal motions of the particles, and since the electrons have greater thermal velocities than the ions the current is predominantly due to electrons.

If the probe potential is made negative relative to V_s the electrons are repelled and the ions are accelerated. The electron current decreases as V_p decreases in Region B, which is called the retarding potential region. Obviously the electron current in Region B is a measure of the energy distribution of the electrons since only those with thermal energy at least as great as the repulsive potential of the probe may strike the probe. For a Maxwellian velocity distribution the electron current density in the retarding potential region is

$$j_e = j_r \exp [e(V_p - V_s)/kT_e] \qquad (2.1)$$

where j_r is the random current density given by kinetic theory as

$$j_r = n_e \bar{v}/4, \qquad (2.2)$$

where n_e is the electron number density and the average electron speed $\bar{v}$ is

$$\bar{v} = (8kT_e/\pi m_e)^{1/2} \quad . \qquad (2.3)$$

In the above k is Boltzmann's constant, T_e is the electron

temperature, and m_e is the electron mass. Equations (2.1), (2.2) and (2.3) form the basis of the classical Langmuir probe theory.

Thus, if the ionic current in the retarding potential region is subtracted, the slope of a semi-logarithmic plot of current versus voltage is simply related to the temperature.

At the point $V_p = V_f$, the probe is sufficiently negative to repel all of the electrons except a flux equal to that of the positive ions, and no net current is collected. An insulated electrode inserted into the plasma would assume V_f (the floating potential) as its equilibrium potential.

If the probe voltage is made positive relative to the plasma, electrons are accelerated to the probe and ions are repelled. Near the probe surface an excess of negative charge (the electron sheath) builds up in a layer until the total negative charge there equals the equivalent positive charge on the probe. Outside the sheath there is very little electric field and the electron current which enters the sheath is that due to thermal motion. Since the area of the sheath is relatively constant with increasing probe voltage (Chen, 1965), we have the fairly flat portion in Figure 2.1, labeled by A. This is the region of saturation electron current. The magnitude of the saturation current is a measure of $n_e(kT_e)^{1/2}$ for a Maxwellian distribution by Equations (2.2) and (2.3).

At large negative values of V_p, almost all the electrons are repelled and we have an ion sheath and the saturation ion current seen in Region C of Figure 2.1. Aside from the disparity in magnitudes due to the difference in thermal velocities the ion saturation current is

similar to the electron saturation current (in the case of no magnetic field) except for one major difference discussed by Chen (1965) in his comprehensive review of electric probe theory. When the ion temperature is not the same as the electron temperature the ion saturation current is not a straight-forward measure of $n_i(kT_i)^{1/2}$, where n_i is the ion number density and T_i the ion temperature.

For accelerating potentials theoretical current-voltage characteristics have been calculated in detail by Mott-Smith and Langmuir (1926). In this case the characteristic is highly sensitive to the size and shape of the electrode. Exact expressions are possible only when the characteristic dimension of the probe is either very large or very small compared to the Debye length. For a small sphere the electron current density in an accelerating potential is

$$j_e = j_r[1 + eV_p/kT_e] \tag{2.4}$$

where j_r is given by Equation (2.2) and V_p is the probe voltage. It is seen that the electron density and temperature are easily obtained.

One of the numerous but well-defined restrictions on the applicability of Langmuir probe theory is that the mean free path for charged particle-neutral collisions be greater than the sheath thickness, so that on the average the collected particles suffer no collisions after entering the sheath. If once again we take the Debye length as indicative of sheath thickness we see from Table 1.1 that the E-region of the ionosphere easily satisfies this criterion. The altitude at which $\lambda_D = \ell$ is about 90 km. Above this altitude the motions are essentially

collisionless for the purposes of probe theory, and therefore Langmuir probe theory applies. The case $\ell > \lambda_D > r_p$ corresponds to a thick sheath and $\ell > r_p > \lambda_D$ represents a thin sheath. With a thin sheath the current is space-charge limited; for a thick sheath the current is orbital-motion limited (Mott-Smith and Langmuir, 1926).

Smith (1965) enumerates the capabilities and the practical problems of Langmuir probe measurements in the ionosphere and outlines the design of a tested probe system.

2.2.2 Gerdien Condensers

Gerdien condenser-type instruments (Chalmers, 1957) have as their basis a theory which treats the motions of the charged particles as mobility-controlled, which assumes a mean free path much shorter than the distance over which the electric field changes appreciably. A cylindrical geometry is generally used and a DC voltage is applied between an outer electrode and an inner, coaxial electrode. For ionospheric applications the instrument is flown through the gas by a rocket. If the electric fields due to the space charge are neglected the current collected can be simply related to the ion number density if: (1) the gas flow rate and aspect are known, or (2) the ionic mobility is known, according to the mode of operation. When the radial motion of the charged particles in the condenser is assumed to be collision-dominated and the effect of the space charge is neglected, the theoretical current-voltage characteristic may be derived. Figure 2.2 shows such a characteristic when the ionized gas consists of one positively charged species, one negatively charged species, and a neutral gas mixture. V is the voltage of the cylinder wall with the inner electrode as a reference.

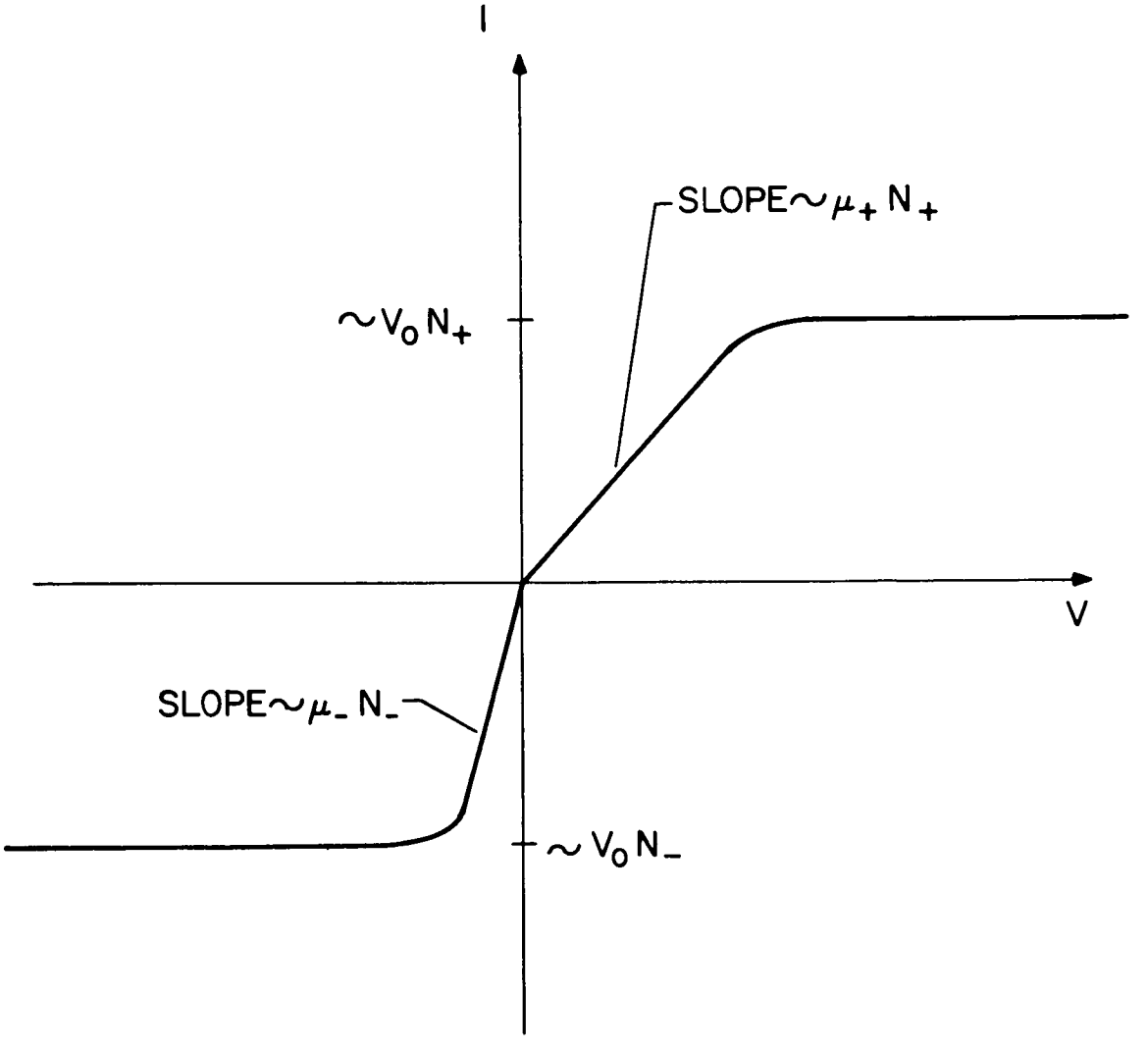

Figure 2.2 Current-voltage characteristics of a Gerdien condenser.

The two flat regions in Figure 2.2 are those of saturation currents. Obviously the maximum current collected is just proportional to the rate of input of ionized gas, or the flow velocity V_o. The saturation currents for singly charged ions are given by

$$(I_s)_{\pm} = N_{\pm} e V_o A \cos \Theta \tag{2.5}$$

where N_+ and N_- are the respective charged particle number densities, A is the right cross-sectional area of the cylinder and Θ is the (small) angle between the cylinder axis and the flow velocity. Subsonic flow is assumed, but in any case the flow rate and the aspect angle must be known to determine the number density.

In the two linear regions of the characteristic the positive and negative currents are given by

$$I_{\pm} = N_{\pm} e C \mu_{\pm} V / \varepsilon_o \tag{2.6}$$

where C is the capacitance of the condenser, ε_o is the permittivity of free space, and $\mu_{\pm}$ are the respective mobilities. Equation (2.6) assumes that the radial drift velocities are proportional to the radial electric field. To determine the number density of either species its mobility must be known.

The assumption that the motion of the charged particles be collision-dominated requires that the cylinder radius be much greater than the mean free path. From Table 1.1 it can be seen that this condition holds for the lowest two altitude regions indicated. Bourdeau, Whipple, and

Clark (1959) have described the results of Gerdien condenser measurements in the altitude range from 35 to 80 km and they discuss many of the practical difficulties encountered, such as those due to complicated air flow patterns and the lack of knowledge of the mobilities of atmospheric ions.

2.3 Motivation for the Present Research

Direct measurement of positive ion concentrations at D-region altitudes is required for a complete understanding of the formation and dynamics of the lower ionosphere. An electrostatic probe carried by a small rocket is a desirable way to make such measurements but the theory of operation of such a probe is as yet incomplete. Any complete theory of positive ion collection in the D-region must take into account the collision-dominated motion of all the particles, the presence of negative ions and electrons, and many instrumental effects. In addition such a probe will probably be in motion through the plasma.

As noted earlier, Langmuir probe theory is not applicable to the D-region because of the short mean free path. Gerdien condenser experiments require knowledge of the air flow through the instrument or of the ionic mobilities to obtain a clear interpretation of the current-voltage characteristic in terms of ionic number densities, all within the framework of a theory which neglects space charge and molecular diffusion (see Section 3.3). Even for number densities as low as 10^3 cm^{-3} the neglect of space charge is probably not justified (Balmain, 1966). Clearly, a more general probe theory is required for D-region applications.

The purpose of the present research is to study the theory of operation of a spherical electrostatic probe immersed in a relatively

high pressure, weakly ionized gas consisting of one type of positive ions, one negatively charged species, and a neutral background gas. The probe is assumed stationary with respect to the plasma. While a complete theory of D-region probes must allow for the possible presence of two or more negatively charged species and a motion of the probe relative to the plasma it is felt that a good understanding of the simplified situation is necessary before undertaking the entire problem.

3. FORMULATION OF THE EQUATIONS GOVERNING A COLLISION-DOMINATED DC PROBE

3.1 Review of the Theory of Boyd

Boyd (1951) explored the possibility of determining the positive ion density from the positive current to a negatively biased spherical probe whose radius is much greater than the mean free path of the plasma in which it is immersed. He noted that the current to the probe is determined by the potential distribution around the probe and divided the space surrounding the probe into four regions (listed here in order of increasing distance from the probe):

(i) the space-charge sheath, in which the positive ion density, $n_+ >> n_-$, where n_- is the negative particle number density. This is a region of strong electric field.

(ii) the "abnormal extra-sheath region", in which $n_+ \approx n_-$ but the electric field is strong

(iii) the "normal extra-sheath region", where $n_+ \approx n_-$ and the electric field is weak

(iv) the undisturbed region.

Outside the abnormal extra-sheath region Boyd used the ordinary mobility relation in which the average particle velocity is proportional to the electric field. Closer to the probe, in the abnormal extra-sheath and the sheath, he employed Sena's high-field mobility (Sena, 1946) in which the average velocity is proportional to the square root of the electric field. While the use of two mobility models is physically well-motivated, Cohen (1963) pointed out the mathematical impossibility of properly matching the solutions for the "normal" region and the "abnormal" region.

By neglecting the ion diffusion term in the flux equation Boyd was able to find the potential profile from solutions to Poisson's equation coupled with the appropriate mobility relation, for the case where the sheath thickness is less than a mean free path. In the opposite limit ($\ell << \lambda_D$) he concluded that the problem was solvable only if the sheath thickness were predetermined by experiment, which is a very severe restriction, both practically and theoretically. The reason for the conclusion was the highly non-linear character of the differential equation for the potential distribution (this equation will be seen later in a more complete form than in Boyd's analysis); and approximate numerical solutions were practically impossible before the advent of the modern digital computer.

3.2 The Theory of Su and Lam

Su and Lam (1963) have developed a continuum theory of spherical electrostatic probes in a dense, slightly ionized gas. They discuss negatively biased probes in a proper mathematical fashion, beginning with Poisson's equation and two flux relations deduced from linear irreversible thermodynamics. Four distinct regions of the disturbance around the probe emerged as a result of their analysis:

(i) the quasi-neutral region

(ii) the transitional region

(iii) the ion sheath

(iv) the ion-diffusion layer.

The ion-diffusion region is a thin layer (thickness $\sim \ell$) immediately adjacent to the probe surface in which the ion diffusion term in the flux equations dominates the mobility term. The outer edge of this

layer joins the ion sheath, in which there are practically no negatively charged particles and $n_+ >> n_-$. Just outside the sheath, in the transitional region, the negative particles become important although still less numerous than positive ions. The inequality varies from $n_+ >> n_-$ to $n_+ \geq n_-$ in this region until, finally in the quasi-neutral, $n_+ \approx n_-$. Boyd's normal extra-sheath corresponds to the quasi-neutral region.

Explicit forms for the current-voltage characteristics were found by Su and Lam for very negative probes and for probes near plasma potential. In both cases the probe radius was assumed to be much greater than the Debye length. Numerical solutions to the equations were constructed for a wider range of probe sizes under another approximation to be discussed in detail in Chapter 4.

3.3 Su and Lam's Equations

The equations developed by Su and Lam (1963) include the effects of space charge in the potential distribution around the probe. They also allow for currents due to free diffusion in the flux relations, and they treat the particle motions as collision-dominated. Thus the physics of the simplified situation described at the end of Section 2.3 in which a spherical DC probe, stationary relative to the plasma, draws a positive ion current should be governed by Su and Lam's equations. Therefore the development of the governing equations in this report follows that of Su and Lam (1963).

From linear irreversible thermodynamics the expressions for the current densities of positive ions and electrons (or negative ions) in a slightly ionized, dense gas are, respectively,

$$\vec{J}_+ = e[-\vec{\nabla}(D_+N_+) - \mu_+N_+\vec{\nabla}V] \tag{3.1}$$

$$\vec{J}_- = -e[-\vec{\nabla}(D_-N_-) - \mu_-N_-\vec{\nabla}V] \quad , \tag{3.2}$$

where N_+, N_-, μ_+, μ_-, D_+, D_-, are the number densities, mobilities, and diffusion constants for the positive and negative species, and V is the electrostatic potential. These expressions can also be derived directly from a kinetic theory point of view in the continuum limit (see Wasserstrom et al. 1965). The first term on the right-hand sides of (3.1) and (3.2) is the current density due to molecular diffusion, and the second term is the electrically-driven (ohmic) current density. In the steady state and with no production or loss of charged particles the two equations of charge conservation become

$$\vec{\nabla} \cdot \vec{J}_+ = 0 \tag{3.3}$$

$$\vec{\nabla} \cdot \vec{J}_- = 0 \quad . \tag{3.4}$$

The electrostatic potential V(r) must obey Poisson's equation (written here in rationalized MKS units):

$$\nabla^2 V(r) = -e(N_+ - N_-)/\varepsilon_o \quad . \tag{3.5}$$

In Equations (3.1), (3.2), and (3.5), singly-charged ions are assumed, and a spherical coordinate system with an origin concentric with the probe are to be used, with r the radial coordinate.

The boundary conditions imposed on this set of equations are that infinitely far from the probe the positive and negative number densities are equal to the quiescent plasma density, N_o, and are zero at the probe surface, $r = r_p$, assuming an absorbing probe surface, and that the potential of the quiescent plasma is taken to be zero and that of the probe to be V_p. That is,

$$N_+(\infty) = N_-(\infty) = N_o \tag{3.6}$$

$$N_+(r_p) = N_-(r_p) = 0 \tag{3.7}$$

$$V(\infty) = 0 \tag{3.8}$$

$$V(r_p) = V_p \tag{3.9}$$

Equations (3.3) and (3.4) may be integrated once. With I_+, the total positive ion current, and I_-, the total negative ion current, as the respective constants of integration we have:

$$4\pi r^2 e\, D_+ \left[\frac{dN_+}{dr} + \frac{N_+ e}{kT_+}\frac{dV}{dr}\right] = I_+ \tag{3.10}$$

$$4\pi r^2 e\, D_- \left[\frac{dN_-}{dr} - \frac{N_- e}{kT_-}\frac{dV}{dr}\right] = I_- \quad , \tag{3.11}$$

where the Einstein relations, $D_+ = \mu_+ kT_+/e$ and $D_- = \mu_- kT_-/e$ have been employed.

To isolate important physical parameters we introduce dimensionless

variables as follows:

$$n_+ = N_+/N_o \quad , \quad n_- = N_-/N_o$$

$$\phi = -eV/kT_-$$

$$s = r/r_p \quad .$$

The negative sign in the definition of ϕ was chosen to make ϕ positive for negatively biased probes. Equations (3.5), (3.10), and (3.11) become

$$\frac{d^2\phi}{ds^2} + \frac{2}{s}\frac{d\phi}{ds} = r_p^2 N_o e^2 (n_+ - n_-)/\varepsilon_o kT_- \tag{3.12}$$

$$\frac{dn_+}{ds} - \frac{n_+}{\varepsilon}\frac{d\phi}{ds} = I_+/4\pi r_p N_o e D_+ s^2 \tag{3.13}$$

$$\frac{dn_-}{ds} + n_- \frac{d\phi}{ds} = I_-/4\pi r_p N_o e D_- s^2 \tag{3.14}$$

where $\varepsilon = T_+/T_-$.

If we now recognize the square of the Debye length, λ_D, in Equation (3.12)

$$\lambda_D^2 = \varepsilon_o kT_-/N_o e^2$$

and the random positive ion current, I_R, (that which would flow if the

probe were at the plasma potential)

$$I_R = 4\pi N_o e D_+ r_p$$

we can make a transformation to simplify Equation (3.12). First, we define the ratio of positive ion current to I_R,

$$\alpha = I_+/I_R \quad . \tag{3.15}$$

Then we introduce the inversion transformation

$$x = \varepsilon\alpha/s \quad . \tag{3.16}$$

Equations (3.12), (3.13), and (3.14) become

$$x^4 \frac{d^2\phi}{dx^2} = (\varepsilon\alpha r_p)^2 (n_+ - n_-)/\lambda_D^2 \tag{3.17}$$

$$\varepsilon \frac{dn_+}{dx} - n_+ \frac{d\phi}{dx} = -1 \tag{3.18}$$

$$\frac{dn_-}{dx} + n_- \frac{d\phi}{dx} = -\mu_+ I_-/\mu_- I_+ \quad . \tag{3.19}$$

Due to this transformation the coordinate of the probe surface is $x = \varepsilon\alpha$, while points infinitely far from the probe correspond to $x = 0$. The boundary conditions (3.6), (3.7), (3.8), and (3.9) become, in the dimensionless variables and the inverted coordinate system:

$$n_+(0) = n_-(0) = 1 \tag{3.20}$$

$$n_+(\varepsilon\alpha) = n_-(\varepsilon\alpha) = 0 \tag{3.21}$$

$$\phi(0) = 0 \tag{3.22}$$

$$\phi(\varepsilon\alpha) = \phi_p = -eV_p/kT_- \tag{3.23}$$

This system of equations is highly nonlinear. The method of solution is discussed in Chapter 4.

4. METHOD SOLUTION FOR HIGHLY NEGATIVE PROBES

4.1 Approximate Analytic Techniques

For highly negative probes ($\phi_p >> 1$) it should be expected that the current of negatively charged particles vanishes. Equation (3.19) becomes

$$\frac{dn_-}{dx} + n_- \frac{d\phi}{dx} = 0 \quad , \tag{4.1}$$

with the simple solution, using (3.20),

$$n_- = \exp(-\phi) \quad . \tag{4.2}$$

Equation (4.2) is the Boltzmann distribution for negative ions in a repulsive potential. It should be valid whenever the negative ion current to the probe is much less than its random value. Su and Lam (1963) discussed this point in detail. They showed (4.2) to be nearly exact for highly negative probes.

As mentioned previously, Su and Lam (1963) found approximate analytic solutions to (3.17), (3.18), and (4.2) for probe potentials approaching negative infinity, in the case where r_p/λ_D approaches infinity. Cohen (1963), in an asymptotic analysis, also found approximate solutions for the case r_p/λ_D approaching infinity, but with a finite probe voltage.

4.2 Su and Lam's Approximation and Numerical Integration

For probes of more moderate size compared to the Debye length, Su and Lam (1963) invoked numerical methods. Before performing a numerical

integration they combined (4.2), (3.17), and (3.18) to obtain

$$x^4 \frac{d^2\phi}{dx^2} = C\left[\frac{1 + \varepsilon(x^4\phi'')'/C}{\frac{d\phi}{dx}} - (1 + \varepsilon)\exp(-\phi)\right], \quad (4.3)$$

where the primes indicate differentiation with respect to the variable x, and C is given by

$$C = (\varepsilon r_p \alpha)^2/\lambda_D^2 \quad . \quad (4.4)$$

The third-order term, $\varepsilon(x^4\phi'')'$, in (4.3) is of some interest. Su and Lam (1963) pointed out that:

(i) it is responsible for the existence of the ion-diffusion layer, and must be included to fulfill the boundary condition on the positive ion density at the probe surface, Equation (3.21), and

(ii) it causes an instability in the numerical integration.

In their numerical solution of (4.3) Su and Lam (1963) dropped the third-order term. They justified this simplification by the following:

(i) their analysis of probes for which

$$\phi_p > \frac{1}{3} \ln[C/(1 + \varepsilon)] >> 1 \quad (4.5)$$

indicated that the decrease in $\phi(x)$ due to neglect of the third-order term is of the order of ε, and is, therefore, negligible for $\phi_p >> 1$

(ii) in many plasmas, $\varepsilon << 1$

(iii) if the term is retained the numerical integration cannot be performed even by modern digital computers.

Also, because of the boundary layer behavior of the positive ion density in the ion-diffusion layer, Su and Lam (1963) claimed that the solutions, $\phi(x)$, of (4.3) are insensitive to the boundary condition, (3.21), on the positive ion density at the probe surface. For these reasons they dropped the third-order term. Numerical integrations of (4.3) could then be performed with C as a free parameter, thus providing potential profiles from which the current-voltage characteristic of the probe could be constructed. The results of this approximation and the subsequent numerical integrations will be presented in Chapter 5 and will be compared to the results obtained by numerical integrations of (3.17), (3.18), and (4.2) in their exact form.

4.3 The Present Work: A Numerical Integration of the Exact Equations

4.3.1 Numerical Solution with no Approximations

In the present work the third-order term is retained for several reasons. First, $\varepsilon = 1$ is the case of interest, since in the D-region $T_+ = T_-$, whether electrons or negative ions are the negative species (Salah and Bowhill, 1966). Also, some approximate numerical solutions by the author indicated that inequality (4.5) would not be satisfied by the parameter C for many normalized currents, α, of interest because r_p/λ_D is of the order of unity in the present problem. Finally, the availability of a very fast digital computer (Illiac II of the Department of Computer Science at the University of Illinois), capable of thirteen-place accuracy, made possible some numerical solutions of (3.17), (3.18), and (4.2), with no approximations.

The general technique employed in the present research was to perform numerical integrations of (3.17) and (3.18), using (4.2), in the

direction of increasing x (toward the probe surface). A Runge-Kutta-Gill routine (Gill, 1951) was used. If the point $x = 0$ could have been chosen as the starting point for the integration, the quasi-neutral solution (which obtains on setting $n_+ = n_-$, and using $\phi(0) = 0$) could certainly have provided initial values for n_+, n_-, ϕ, and the derivative of ϕ, thus determining the necessary starting values for the integration. However, due to the behavior of the second derivative of ϕ at $x = 0$, a small but non-zero value of x had to be chosen as the starting point. A correction term to the quasi-neutral solution was necessary, and compatible starting values for x, n_+, n_-, ϕ, and ϕ' were required. The Poincare-Lighthill-Kuo technique (Tsien, 1956) was used to find these values (see Appendix A). Then for $\varepsilon = 1$, values were chosen for α and r_p/λ_D, and a numerical integration was attempted. The integration was to continue to x_p, the coordinate of the probe surface, with the probe potential and the potential profile as the major result. Profiles of $n_+(x)$ and $n_-(x)$ were also to be found.

As expected, this numerical procedure was unstable; it exhibited great sensitivity to the starting value, ϕ_o', of the derivative of the potential. The normalized positive ion density, $n_+(x)$, increased rapidly with x if ϕ_o' was too high; if ϕ_o' was too low, $n_+(x)$, took on negative values. Tests for these instabilities were incorporated into the computer program (see Appendix B). Thus the problem was to determine the correct value (essentially an eigenvalue) of ϕ_o' accurately enough for the integration to proceed to x_p in a stable manner. An iterative process in the computer program (see Appendix B) was used to find this eigenvalue. The integration was terminated at the probe surface and the value of

$n_+(x_p)$ was examined. If $n_+(x_p)$ was greater than zero the numerical integration was repeated with a slightly lower value of ϕ_o' in an attempt to match $n_+(x_p)$ to zero. The value of ϕ_o' was repeatedly adjusted in this manner by an iterative routine in the computer program until either $n_+(x_p)$ was matched to zero, or ϕ_o' was determined to the limits of machine accuracy (thirteen decimal places). It was difficult to obtain numerical solutions in this way for many values of interest of the parameter C, the larger C, the more difficult. For $C > 50$, the starting value for ϕ_o' had to be determined more precisely than to thirteen decimal places, the precision limit of the computer, and numerical solutions were impossible. For $C < 50$, solutions were possible but the probe potentials of these solutions were not large enough to allow the construction of the current-voltage characteristic of the probe for practical voltages ($\phi_p > 150$, or $V_p < -0.75$ volts for $T_- = 210°K$).

This approach evidently could not generate the current-voltage characteristic of the probe over a wide range of operating conditions, but it illustrated the behavior of the exact solutions and thus inspired the development of a more effective technique (see Section 4.3.2). The concentrations of positive and negative ions around the probe, obtained entirely by the numerical integration, are shown in Figure 4.1 for $r_p/\lambda_D = 0.64$ and $\alpha = 8.50$.

In the numerical computations the independent variable was scaled according to

$$\bar{x} = x/(1 + \varepsilon) \quad . \tag{4.6}$$

This scaling was introduced to reduce the computer time required for

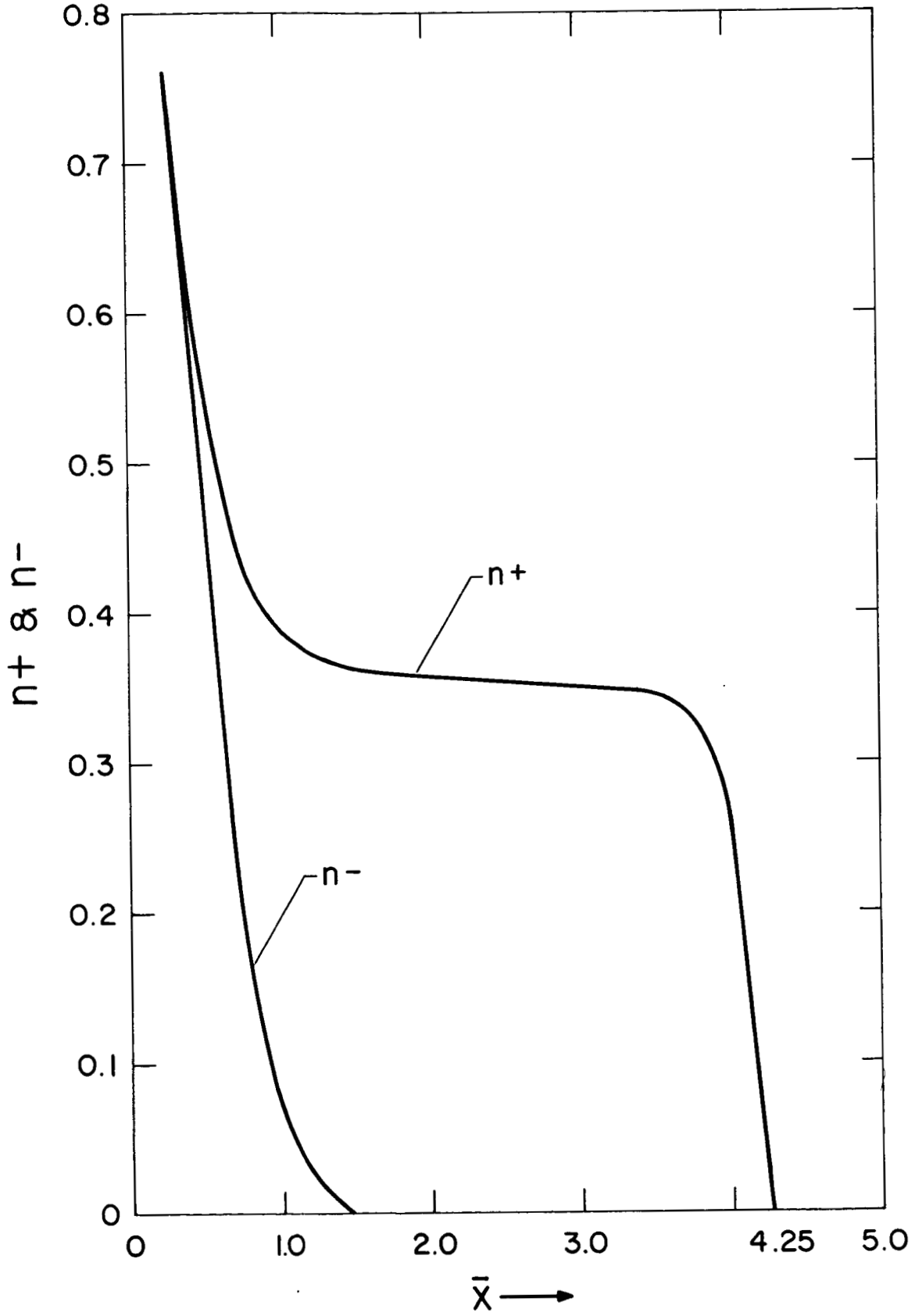

Figure 4.1 Positive and negative ion densities obtained by a numerical integration.

the numerical integration and to facilitate direct comparison with the results of Su and Lam (1963), since they used the same scaling in their numerical solutions of the simplified form of (4.3). Here, $\varepsilon = 1$ is adopted; Figure 4.1 is therefore a plot of n_+ and n_- versus $\bar{x}$. The four regions described by Su and Lam (1963) are seen clearly. Between the probe surface, $\bar{x}_p = 4.25$, and $\bar{x} = 3.5$ the ion-diffusion layer appears. The thickness of this layer, by (3.16), is approximately $0.2\ r_p$. The ion sheath, $1.5 \leq \bar{x} \leq 3.5$, is striking in that the ion density there is nearly constant. This feature will be discussed in more detail. At the outer edge of the sheath we see the transitional region and then the quasi-neutral region ($x < 0.5$). The starting point for the integration, $x = 0.25$, corresponds to $r = 17\ r_p$. The probe potential corresponding to the ion distributions in Figure 4.1 is $\phi_p = 21.16$. Successive iterations, which ultimately satisfied the homogeneous boundary condition, (3.21), revealed that the solutions to the equations are quite insensitive to this boundary condition, as predicted by Su and Lam (1963).

The flat portion of the $n_+(\bar{x}_p)$ profile in Figure 4.1 which will be called the "uniform sheath region", was a common feature of all the solutions obtained when the equations were solved with no approximations. The existence of this region served as the basis for a more powerful method of solution of (3.17) and (3.18), in which the numerical integration could be terminated before reaching the probe surface, and matched to an approximate analytical solution. The next section explains this method.

4.3.2 Matching an Approximate Analytic Solution to an Incomplete Numerical Solution

A simple but extremely accurate approximation led to a more feasible numerical technique. Re-writing (3.17) and (3.18) in the $\bar{x}$-coordinate system, and substituting for n_- from (4.2) we have, again for $\varepsilon = 1$,

$$\bar{x}^4 \frac{d^2\phi}{d\bar{x}^2} = C[n_+ - \exp(-\phi)]/4 \quad , \tag{4.7}$$

and

$$\frac{dn_+}{d\bar{x}} = n_+ \frac{d\phi}{d\bar{x}} - 2 \quad . \tag{4.8}$$

The simplification arose from noticing that the second derivative, ϕ'', of the potential, rapidly approaches zero as $\bar{x}$ increases. Thus the potential gradient, ϕ', approaches an asymptote which is just the value of ϕ' at the probe surface. Let K be the asymptote; then for values of $\bar{x}$ larger than $\bar{x}_o$ (the point at which ϕ'' becomes arbitrarily small),

$$\frac{dn_+}{d\bar{x}} = Kn_+ - 2 \quad . \tag{4.9}$$

The solution to (4.9) is, for $\bar{x} > \bar{x}_o$,

$$n_+ = 2(1-\exp[-K(\bar{x}_p-\bar{x})])/K \quad , \tag{4.10}$$

which describes the behavior of $n_+(\bar{x})$ in Figure 4.1 for $\bar{x} > 2.0$. We may not neglect the exponential term compared to unity in (4.10) when

$$\exp[-K(\bar{x}_p-\bar{x})] > 10^{-2} \tag{4.11}$$

Inequality (4.11) may be considered the defining relation for the extent of the thin ion-diffusion layer. In the numerical integration which produced Figure 4.1 the asymptotic value for ϕ' was $K\approx 5.80$, and $\exp[-K(\bar{x}_p-\bar{x})]\approx 10^{-2}$ at $\bar{x} = 3.50$. When $\exp[-K(\bar{x}_p-\bar{x})] < 10^{-2}$, $n_+\approx 2/K$, which is seen to be a good approximation to the nearly uniform ion density in the sheath.

Now for highly negative probes n_- may be neglected compared to n_+ in the sheath. This is seen in Figure 4.1 for the case $\phi_p = 21.16$, which is not a particularly large probe potential. This neglect was also justified analytically by Su and Lam (1963). Therefore, (4.10) may be substituted into (4.7) to obtain an expression for ϕ'' in the sheath:

$$\bar{x}^4 \frac{d^2\phi}{d\bar{x}^2} = C/2K \quad . \tag{4.12}$$

The differential equation (4.12) for the potential applies between $\bar{x}_o$ and the outside edge of the diffusion layer, where (4.11) holds and the equation becomes

$$\bar{x}^4 \frac{d^2\phi}{d\bar{x}^2} = C(1 - \exp[-K(\bar{x}_p-\bar{x})])/2K \quad . \tag{4.13}$$

The best justification for these simplifications is the results of the integrations described in Section 4.3.1 in which it was attempted to carry the numerical integration all the way to the probe surface. For

the prescribed range of values of r_p/λ_D

$$0.1 < r_p/\lambda_D < 1.0 \quad , \tag{4.14}$$

highly negative probes always yielded solutions for which the regions of disturbance around the probe were exactly as found by Su and Lam (1963). In particular, a sheath of nearly uniform ion density always appeared; the transitional region was never adjacent to the ion-diffusion layer. In addition, the potential gradient always approached its asymptotic value (to better than one part in 10^3) before the integration reached the probe surface.

Consequently the procedure used to generate the current-voltage characteristics of the probe from (4.7) and (4.8) was to choose values for the parameter C and numerically integrate (4.7) and (4.8) up to $\bar{x}_o$, the point where the second derivative of the potential became arbitrarily small ($\phi'' = 10^{-2}$ was chosen). Then (4.12) produced analytic solutions valid up to the diffusion layer, which were matched to the numerical solutions at $\bar{x}_o$, the point of termination of the latter. In this region the potential obeys

$$\phi(\bar{x}) = \phi(\bar{x}_o) + K(\bar{x} - \bar{x}_o) + 10^{-2} \int_{\bar{x}_o}^{\bar{x}} (\bar{x})^{-3} d\bar{x} \quad . \tag{4.15}$$

(4.15) is nearly exact. The integral term represents the correction due to the non-zero value of ϕ'' at $\bar{x}_o$ ($\phi''(\bar{x}_o) = 10^{-2}$). In all cases of interest, its magnitude was less than 3×10^{-3} times the magnitude of the first two terms on the right side of (4.15).

A range of values of $\bar{x}_p = \alpha/2$ for each C were found by (4.14) and the criterion (4.11) applied to find the edge of the diffusion layer, in which (4.13) must be used in place of (4.12). It was found that the resulting expression for $\phi(\bar{x})$ in the diffusion layer produced a negligible change in the probe potential, ϕ_p, from that resulting from the application of (4.15) all the way to the probe surface, for all values of K from the numerical integrations and for all $\bar{x}_p$ from (4.14). This verifies the conclusion found earlier by exact numerical integration, that the boundary condition (3.21) on the positive ion density at the probe surface does not appreciably affect the solution.

The method of solution just outlined takes advantage of the asymptotic behavior of ϕ' and thus permits a numerical solution of (4.7) and (4.8); it avoids the instability which would beset a numerical integration carried into the ion-diffusion region. The results of this integration is given in Chapter 5.

5. RESULTS AND DISCUSSION

5.1 Some Results of the Present Work and Comparisons to Those of Su and Lam

The probe equations, (4.7) and (4.8), were solved by the method described in Section 4.3.2. The solutions were tested for sensitivity to variations in the step size and the initial values by repeating the numerical integration with different starting values and step size. If the solution obtained with the original parameters agreed with that obtained using the new parameters to at least three significant figures the solution was accepted. The step size ultimately chosen was 0.01, and in most cases, the solutions agreed to at least four places when tested for sensitivity. These solutions are presented here and compared to those obtained numerically by Su and Lam (1963) for probes of moderate size (see Sections 4.1 and 4.2). Su and Lam performed numerical integrations of Equation (4.3) after dropping the third-order term and using the scaling of (4.6). For $\varepsilon = 1$ the equation they solved was

$$\bar{x}^4 \frac{d^2\phi}{d\bar{x}^2} = C\,[1/\frac{d\phi}{d\bar{x}} - \exp(-\phi)]/2 \quad . \qquad (5.1)$$

As noted in Section 4.3.2 the potential gradient very closely approaches its asymptote well before the integration reaches the $\bar{x}$-coordinate of the probe surface. Figure 5.1 shows this asymptote, K, as a function of the parameter, C. The upper trace was obtained by integrating (4.7) and (4.8). The lower trace was found by the present author's numerical integrations of (5.1) and agrees with that obtained by Su and Lam. For $C^{1/2} \gtrsim 7.0$ both curves display the linear dependence of K on $C^{1/2}$ as predicted theoretically by Su and Lam, but their neglect of the third-order

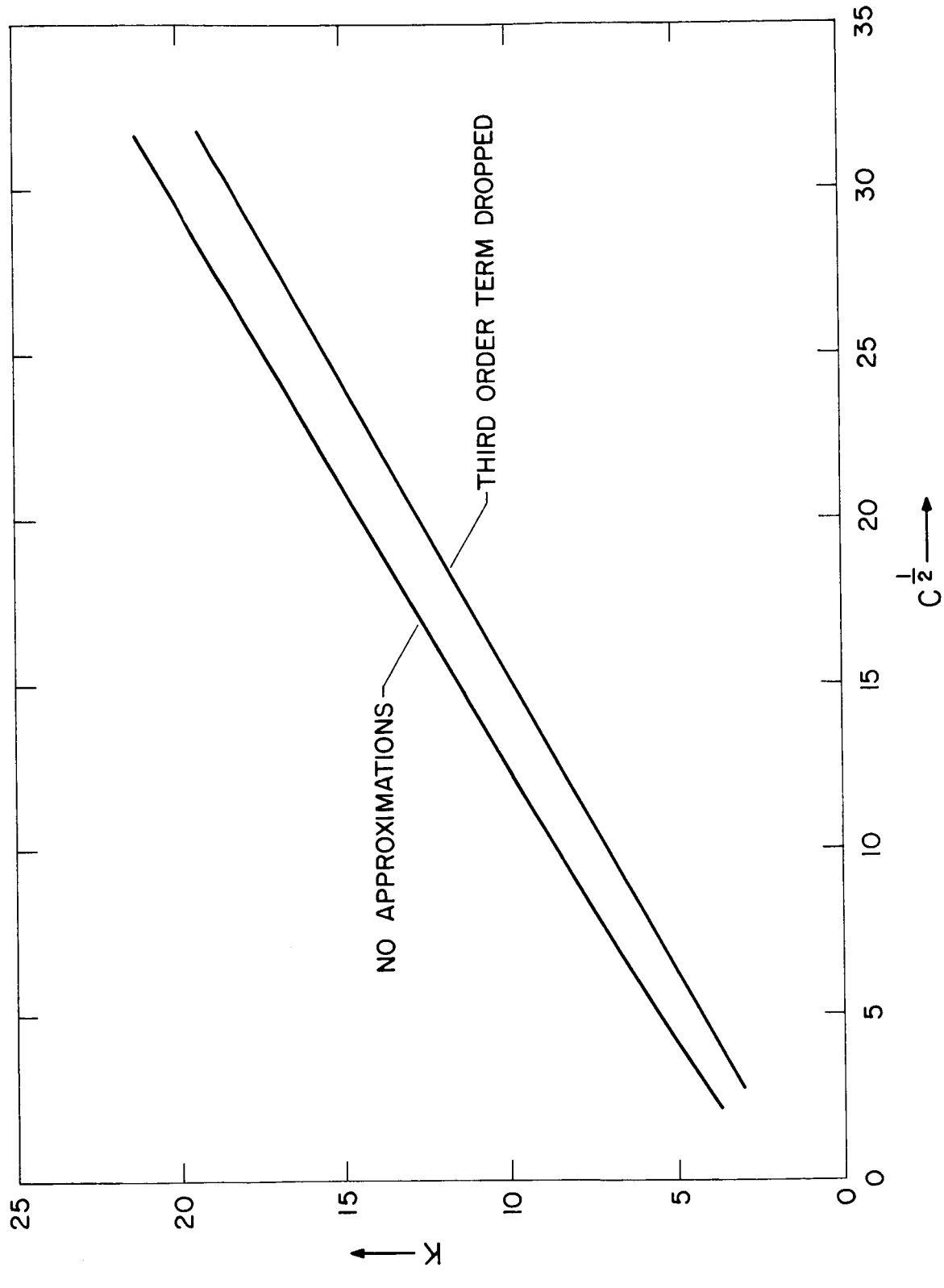

Figure 5.1 Asymptotic value of $\frac{d\phi}{dx}$ as a function of the parameter, C.

term evidently yields values of K lower than the true curve. Therefore, to collect a given current (a given $\bar{x}_p$), a probe voltage higher than that predicted by Su and Lam is required, by an amount depending on the current and the ratio r_p/λ_D. A direct physical explanation of this effect has not been found; it should be noted that the neglect of the third-order term was not an assumption based solely on physical grounds. Mathematically, the third-order term is necessary for the existence of the ion-diffusion layer (actually a boundary layer for n_+). Indeed, the approximation leaves only the Equation (5.1), and the positive ion density must be found by applying Poisson's equation to the numerically computed potential profile.

Figure 5.2 illustrates the resulting positive ion density distribution for a representative situation, C = 140, $r_p/\lambda_D = 0.5$. Also in Figure 5.2, in great contrast, is the positive ion distribution calculated from (4.7) and (4.8) by the technique of Section 4.3.2. It plunges to zero extremely rapidly in the ion-diffusion layer. While both positive ion density profiles in Figure 5.2 are nearly constant in the sheath ($2.0 < \bar{x} < 11.5$) the number density found by Su and Lam's approximation is nearly two orders of magnitude too small. Therefore, it must be concluded that the neglect of the third-order term in (4.3) seriously affects the distribution of positive ions around the probe. On the other hand, the solution of (4.7) and (4.8) in their exact form prohibits large negative gradients of $n_+(\bar{x})$ in the quasi-neutral and transitional regions, $\bar{x} < 2.0$. It is important that the true ion distribution be known for any extension of the theory of the stationary probe to moving probes.

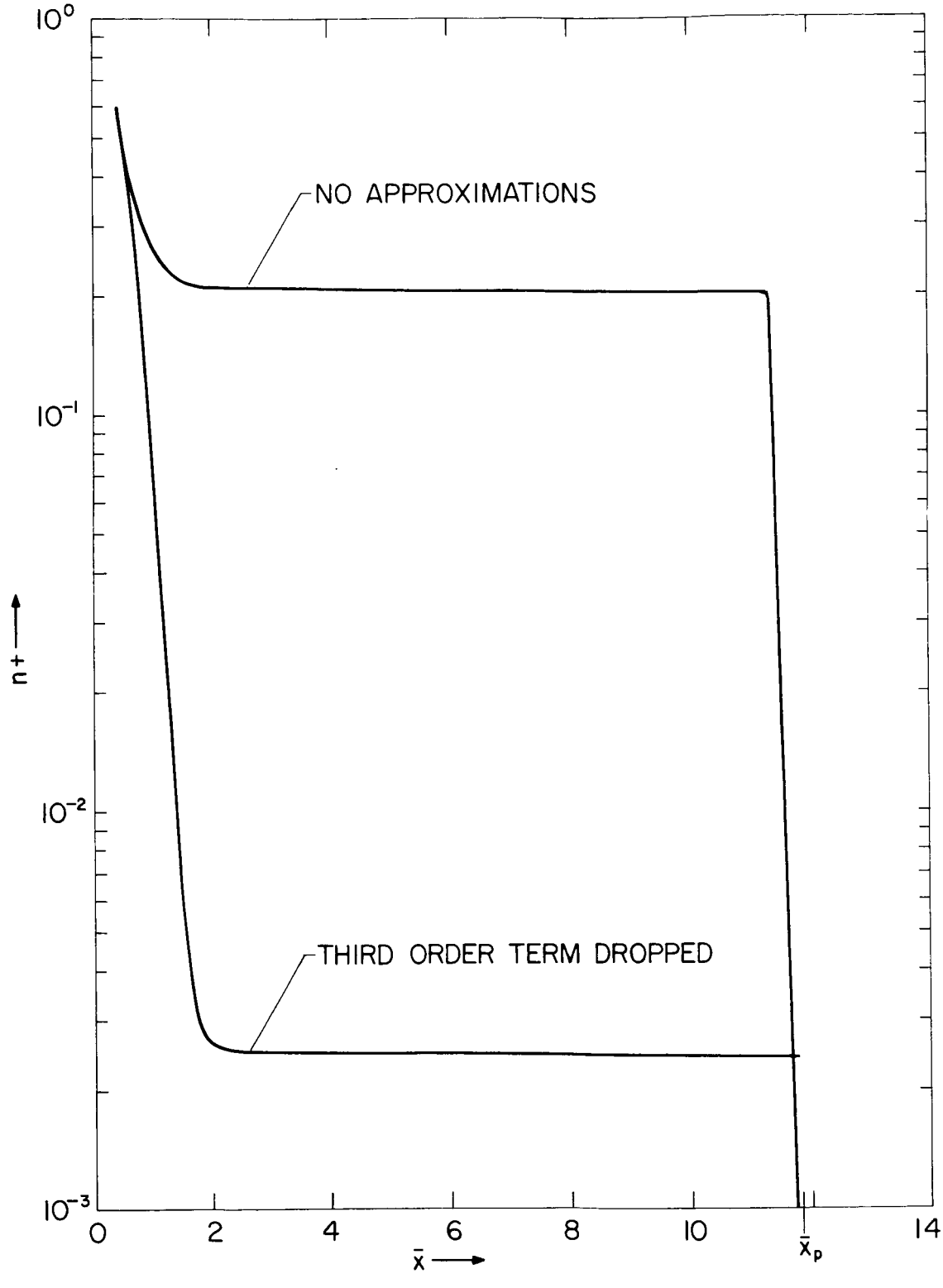

Figure 5.2 Positive ion distributions from the numerical integrations.

5.2 Potential Profile and the Current-Voltage Curves

Figure 5.3 shows the potential distributions around the probe for various values of C, calculated by numerical integration of (4.7) and (4.8). Within the sheath it is seen that $\phi(\bar{x})$ is nearly linear in $\bar{x}$, which implies that $\phi(r) \sim r^{-1}$, and the disturbance of the probe extends well into the plasma, at least ten probe radii for the $\bar{x}_p$ values of interest. Therefore, no saturation should be expected in the current-voltage characteristic of the probe, although as Cohen (1963) stated, a tendency toward saturation exists for very large probes ($r_p/\lambda_D \to \infty$). This nearly r^{-1} dependence of ϕ should not, however, be taken as an indication that the potential distribution is the same as that which would exist in free space. In fact, the electric field in the ion-diffusion layer and the sheath is significantly larger than the field which would exist if space charge were negligible, typically 1.1 or 1.2 times as large for the values of C indicated in Figure 5.3 and the values of $\bar{x}_p$ from (4.4) and (4.14). This can be seen by comparing the electric field, E, from the numerical integrations, with the electric field, E_o, which would surround the probe if space charge could be neglected. Ignoring the vector nature of the fields since both E and E_o have only a radial component (which is negative), $E = \frac{dV}{dr} = \frac{dV}{d\bar{x}} \frac{d\bar{x}}{dr} = \bar{x}_p kTr_p \left(\frac{d\phi}{d\bar{x}}\right)/er^2$, and $E_o = kTr_p V_p/er^2$. Therefore,

$$E/E_o = \bar{x}_p \left(\frac{d\phi}{d\bar{x}}\right)/\phi_p \quad . \tag{5.2}$$

The quantity $\frac{d\phi}{d\bar{x}}$ was printed by the computer program (see Appendix B) as a function of $\bar{x}$, thus permitting a plot of the normalized electric field, E/E_o, as a function of distance from the probe.

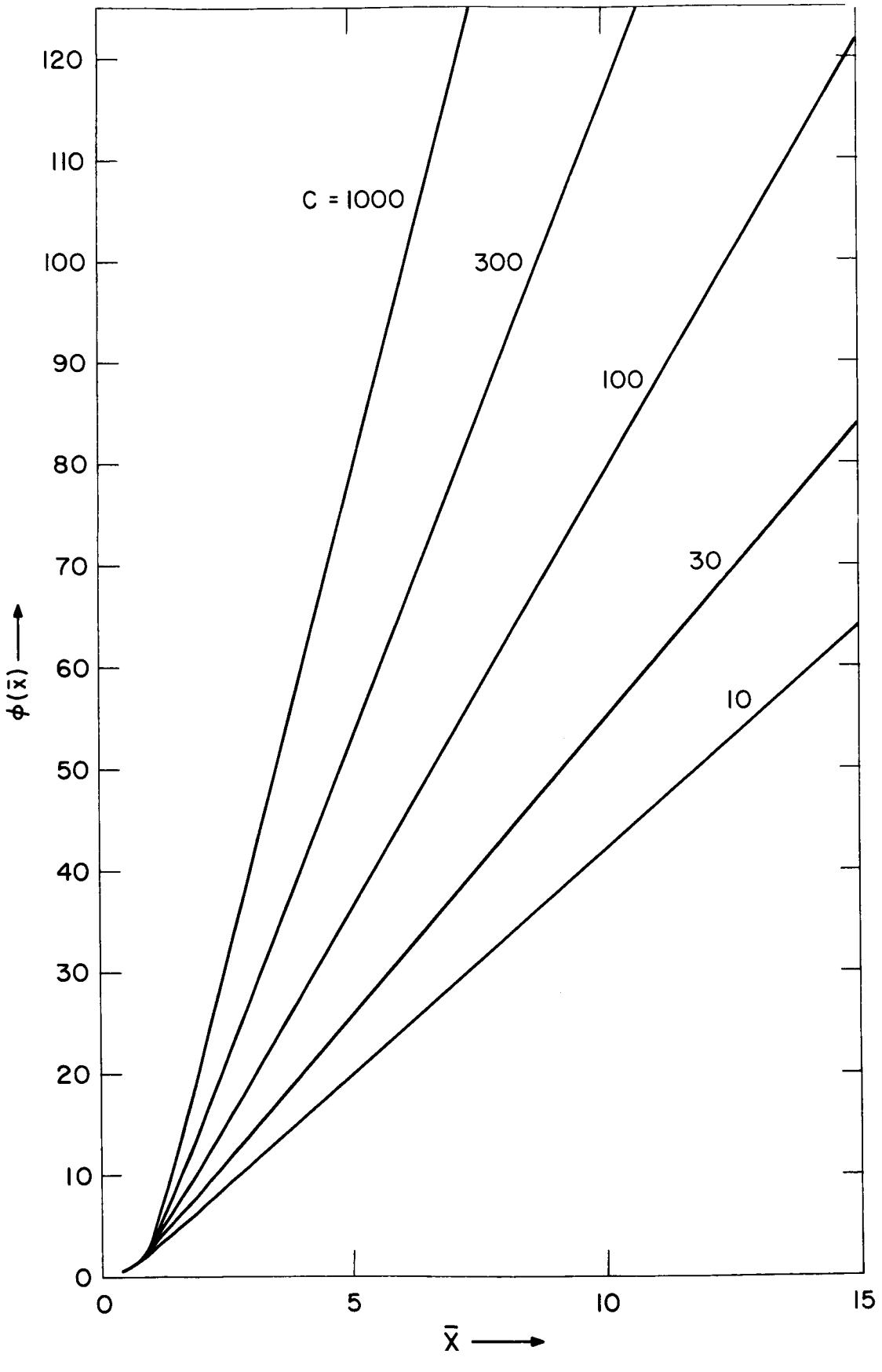

Figure 5.3 Potential distribution around the probe for various values of C.

In Figure 5.4, E/E_o is plotted versus the normalized distance, ρ, from the center of the probe, where $\rho = (r/\lambda_D) = (C^{1/2}/2\bar{x})$. This plot is for C = 100 and $\rho_p = (r_p/\lambda_D) = 0.5$. The probe potential corresponding to this solution is $\phi_p = 79.22$.

Several conclusions may be drawn from Figure 5.4. First, it is apparent that the shielding effect of the positive-ion sheath causes the field to be greater than E_o for $r < 3.5\lambda_D$, or for $(r-r_p) < 3\lambda_D$ since $r_p = 0.5\lambda_D$.

Farther from the probe, for $r > 10\lambda_D$, the ratio E/E_o decreases very slowly with increasing distance. This implies that the field surrounding the probe varies as r^{-2} at large distances from the probe, which just states that the space-charge sheath is of finite extent. For the case shown in Figure 5.4 the space charge is confined to the region $r \lesssim 10\lambda_D$.

Cohen (1963) pointed out that the ratio E/E_o should approach a constant when ρ becomes very large compared to unity, for highly negative probes. Thus, the potential decays only as ρ^{-1} as $\rho \to \infty$ and the Debye shielding in the space-charge sheath (see e.g. Jackson, 1963) is incomplete; the potential around a test particle, which collects no current, decays as $e^{-\rho}/\rho$.

Since the electric field around the probe penetrates far into the plasma, one should not expect the positive-ion current to attain a saturation value. This is in contrast to the behavior of the electron current in Region A of Figure 2.1, the current-voltage characteristic of a Langmuir probe.

The current-voltage characteristics of the probe will now be presented. In Section 3.3, ϕ_p was defined as $-eV_p/kT_-$, and $\bar{x}_p$ as $I_+/2I_R$

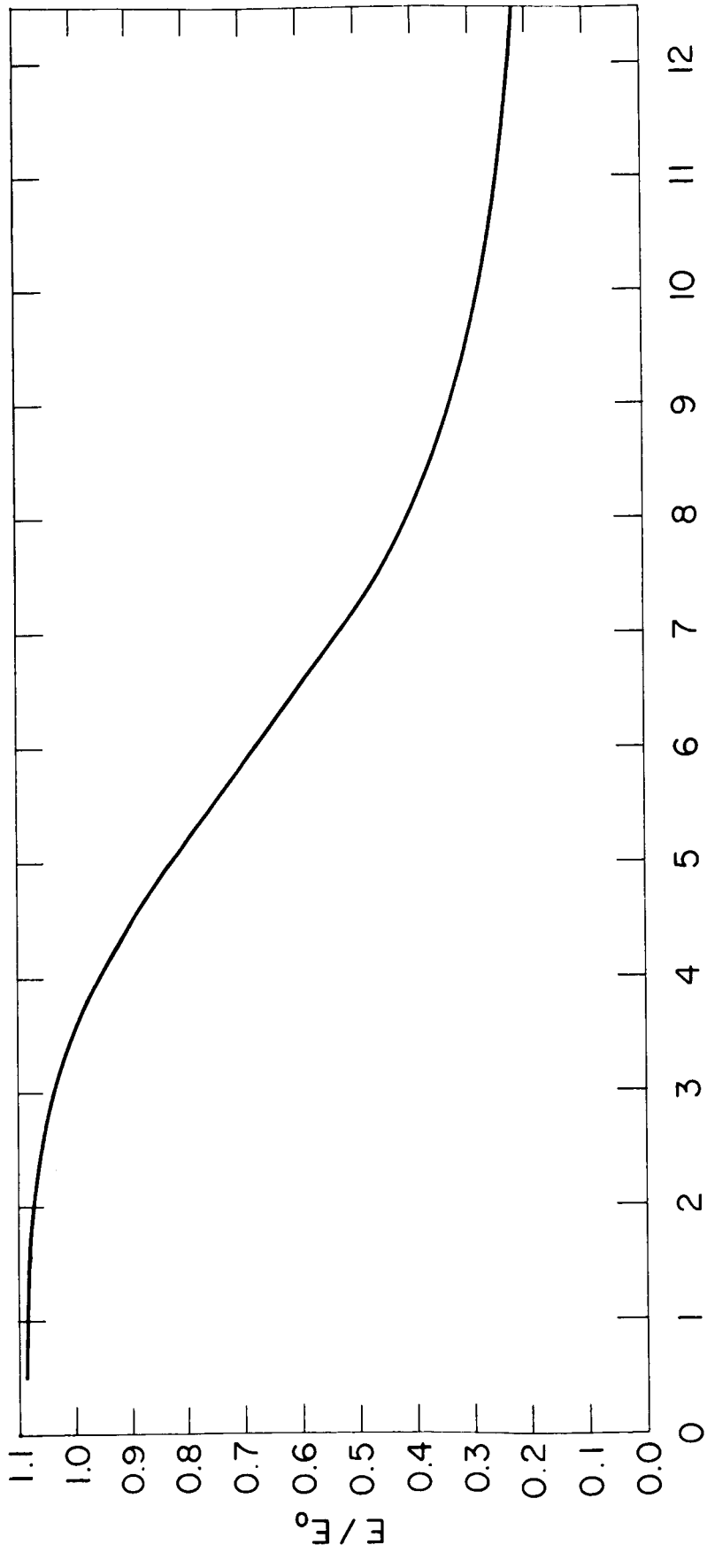

Figure 5.4 Normalized electric field versus the normalized distance from the center of the probe.

(also see Section 4.6), where I_R is the random positive ion current to the probe. Therefore a plot of $\bar{x}_p$ versus ϕ_p may be considered a graph of normalized current versus normalized probe voltage. Curves of $\bar{x}_p$ versus ϕ_p with $\rho_p = (r_p/\lambda_D)$ as a parameter are shown in Figure 5.5. It should be noted, however, that $\bar{x}_p$ is proportional to $(N_o)^{-1}$, from the expression for I_R in Section 3.3.

To display a current independent of the quiescent plasma number density, the quantity $(C/2\bar{x}_p) = (I_+/I_R)\rho_p^2$ is plotted as a solid line versus ϕ_p in Figure 5.6, again with ρ_p as a parameter. Since $(I_+I_R)\rho_p^2$ is proportional to r_pI_+/μ_+, the number density of positive ions may be found from Figure 5.6 in an experiment in which the gas temperature and the positive-ion mobility are known. As expected, the curves of Figure 5.6 have no saturation region, although the curves for higher ρ_p are flatter.

The curves of Figure 5.6 are plotted again in Figure 5.7, but on log-log paper. Again noting that the quantity $(C/2\bar{x}_p)$, on the vertical axis, is proportional to the positive ion current, I_+, and that ϕ_p, on the horizontal axis, is the normalized probe voltage, one may deduce the functional dependence of I_+ on the probe voltage. For $\phi_p > 25$ the traces are linear and therefore

$$I_+ \sim \phi_p^{\beta} \tag{5.3}$$

where β is the slope of the trace. As noted in the discussion of Figure 5.6, the higher ρ_p, the flatter the curves. In fact, for $\rho_p = 1.0$, $\beta = 0.53$, while for $\rho_p = 0.4$, $\beta = 0.55$, and for $\rho_p = 0.1$, $\beta = 0.62$. The

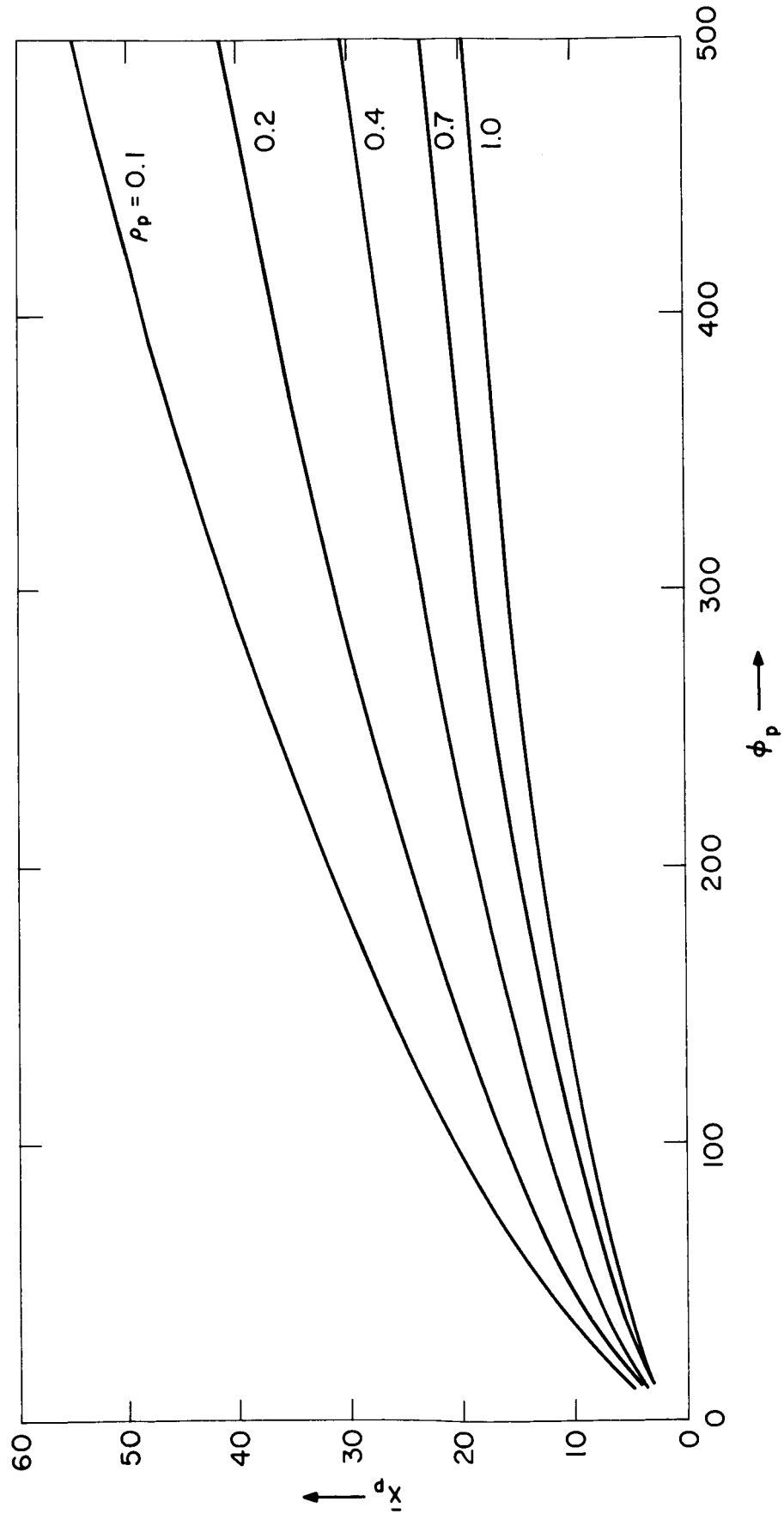

Figure 5.5 Normalized current versus normalized probe voltage with ρ_p as a parameter.

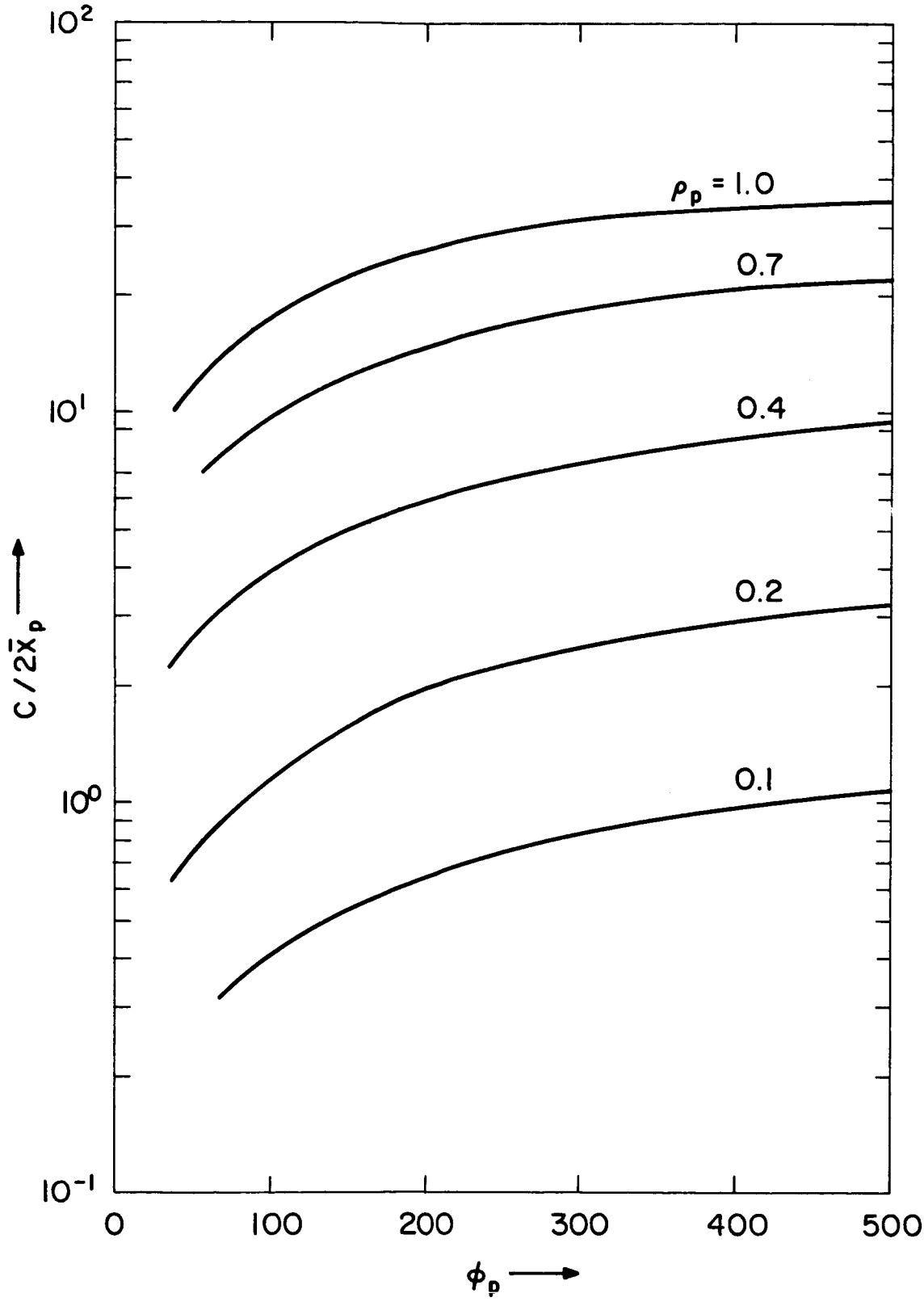

Figure 5.6 Current-voltage characteristics of the probe, I.

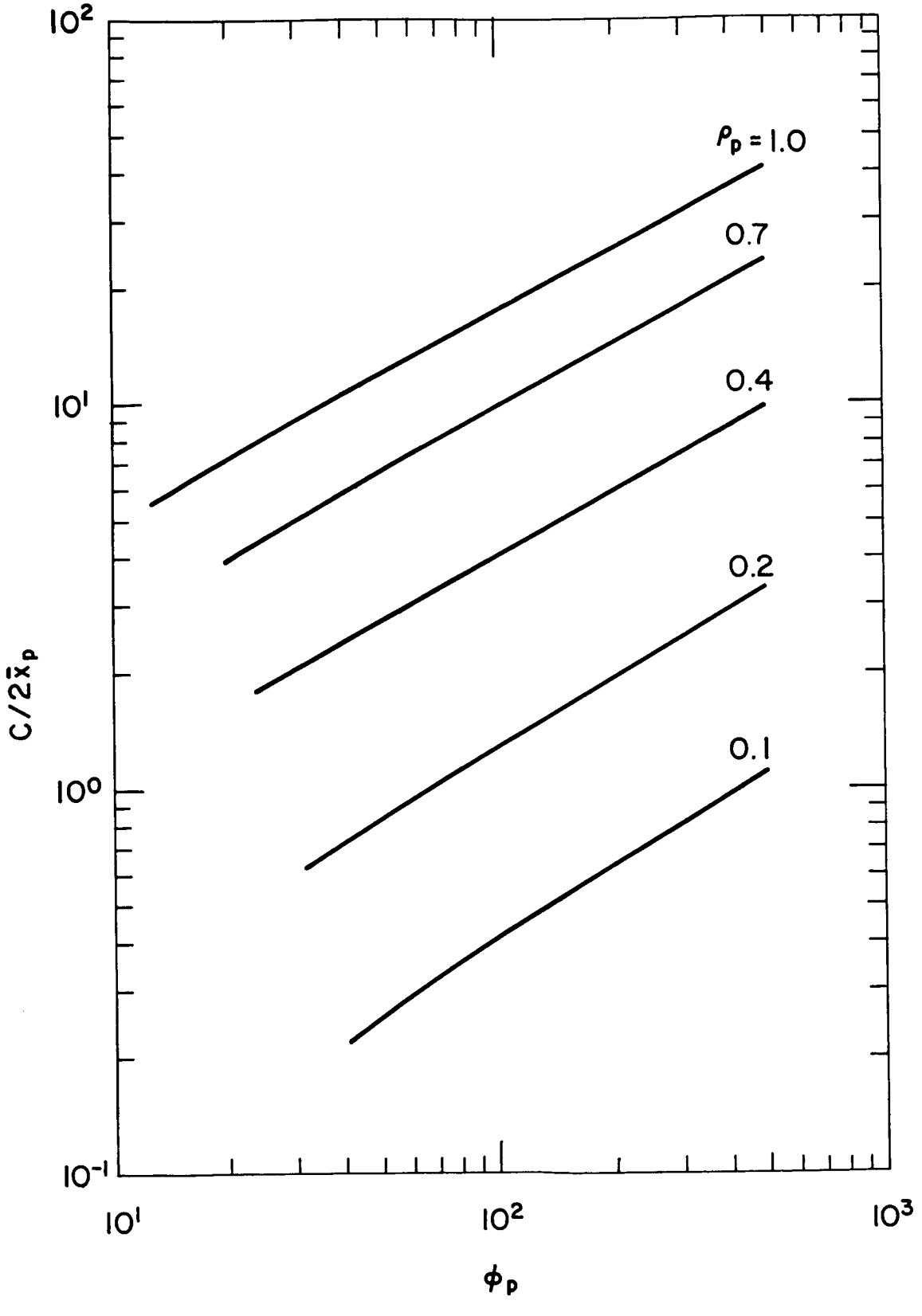

Figure 5.7 Current-voltage characteristics of the probe, II.

fact that β decreases with increasing ρ_p confirms Cohen's (1963) observation, mentioned at the beginning of Section 5.2.

5.3 Comparisons to Simplified Theories

5.3.1 Zero Space Charge Theory

To estimate the importance of including space charge in the theory one may attempt to formulate a theory which neglects it. With no space charge the potential profile in the plasma is the same as in free space, that is,

$$V(r) = r_p V_p / r \tag{5.4}$$

and

$$E = r_p V_p / r^2 \tag{5.5}$$

for $r \geq r_p$. For a highly negative probe one need only consider the positive-ion current. Assuming a steady state and no production or loss of positive ions, Equation (3.3) implies that $I_+ = N_+ e v_+ 4\pi r^2$, where v_+ is the speed of a positive ion; we assume $v_+ = \mu_+ E$. Then by (5.5) we have

$$I_+ = 4\pi r_p e N_+ \mu_+ V_p \quad . \tag{5.6}$$

Thus, a linear relation between the positive ion current and the probe voltage is predicted in a zero space-charge theory. As was pointed out at the end of Section 5.2, the true current-voltage curves obey a relation of the form of (5.3) with $\beta < 1$, and space charge may not be neglected.

5.3.2 Collisionless Theory Including Space Charge

The classical Langmuir probe neglects collisions but considers the effect of space charge. The case of a sheath thin compared to the probe

radius (space charge-limited current) is not of interest in the present study due to the inequality (4.14) and an expression derived by Su and Lam (1963) for the ratio of sheath thickness to probe radius for highly negative probes. For thick sheaths (orbital motion-limited current), the positive ion current to a highly negative spherical probe is given by $4\pi r_p^2$ times the right side of (2.4) with the ion parameters, N_+, m_+, and $T_+(=T_e)$ instead of those of the electron (Boggess, 1959), that is,

$$I_+ = 4\pi r_p^2 N_+ e(kT/2m_+)^{1/2}(1+eV_p/kT_+) \qquad (5.7)$$

For highly negative probes, $-(eV_p/kT_+) = \phi_p >> 1$ and (5.8) reduces to $I_+ \sim \phi_p$, which is not the functional form of the curves of Figure 5.6.

6. INTERPRETATION AND POSSIBLE EXTENSIONS

6.1 Conclusion

The differential equations governing positive ion collection by a spherical probe in a collision-dominated plasma were developed in Chapter 3 and were solved exactly by a numerical technique outlined in Chapter 4 for the case of a highly negative probe. The results of the numerical solution for probes of moderate size compared to the Debye length were presented in Chapter 5. It was shown that the approximation introduced by Su and Lam (1963) appreciably affects the current-voltage characteristics of the probe and leads to a distribution of positive ions around the probe which is very different from the distribution obtained by an exact solution of the equations.

The positive-ion sheath was found to be uniform; the density of positive ions in the sheath was nearly constant. This feature of the space charge distribution permitted the exact solution of the equations in a wider regime of operation of the probe than would have been possible otherwise.

In Section 5.3 the results of the exact solution of the equations were compared to those from simplified theories. It was found that the neglect of space charge is not justified.

6.2 Limitations

Several physical assumptions place limitations on the validity of the equations developed in Chapters 3 and 4. Beginning with Equations (3.1) and (3.2) the assumption was made that the drift velocities of the charged particles are proportional to the electric field, $\vec{E}$, with the appropriate mobility as the proportionality constant. For large electric

fields this assumption breaks down (Sena, 1946). For example, with N_2^+ ions in N_2 gas the drift velocity is proportional to $\vec{E}^{0.6}$ when the ratio of electric field strength to gas pressure is greater than 40 volts/cm/mmHg (McDaniel, 1964). Balmain (1966) stressed the need for a study of ion collection which assumes a drift velocity proportional to $\vec{E}^{\beta}$ where $0.5 \leq \beta \leq 1.0$, in accord with experimental data (McDaniel, 1964). The complications which would arise in such a study are likely to be prohibitive (Cohen, 1963). The applicability of mobility theory throughout the D-region of the ionosphere is not universally accepted. Hoult (1965) justified the use of a simple mobility relation (drift velocity $\sim \vec{E}$) up to 80 km for probe voltages of several volts.

The assumption of a steady state plasma could break down for probe voltages greater than the ionization potentials of the neutral molecules due to the ionization of the neutral gas by the accelerated ions. For D-region temperatures, $kT/e \simeq 2.10^{-2}$ volts, so that $\phi_p = 500$ corresponds to a probe voltage of about 10 volts, high enough to ionize nitric oxide, but less than the ionization potentials of molecular oxygen and molecular nitrogen.

For D-region plasma probes the assumption that the gas is weakly ionized presents no problem (see Section 1.2). A recent paper by Su and Sonin (1967) extends the theory of operation of spherical electrostatic probes to moderately ionized dense gases, at least for the case $r_p/\lambda_D \gg 1$.

It should also be mentioned that the use of the Einstein relations in (3.10) and (3.11) assumed no temperature gradients in the plasma. Magnetic fields were also neglected.

6.3 Possible Extensions

6.3.1 Improvements to the Stationary Probe Theory

A useful extension of the theory of the stationary probe would be the inclusion of two or more positive and negative ion species. It would be especially desirable to allow for the simultaneous presence of electrons and negative ions (see Section 1.2). In this case a third term would be added to the right side of Poisson's equation, (3.5), and an additional flux relation would be necessary. For highly negative probes one would assume that both the electrons and negative ions would be in thermal equilibrium with the repulsive potential of the probe, and their distributions would take the form of (4.2). The condition that the charged-particle gases have the neutral gas temperature would make the problem tractable.

Experimental verification of the theoretical current-voltage curves, Figure 5.6, is not possible in contemporary laboratory plasmas since the fraction of ionization is too high. Also, the appreciable difference between the neutral gas temperature and the charged-particle temperature would alter the curves in Figure 5.6 although current-voltage curves can be generated numerically for arbitrary values of the temperature ratio, ε.

6.3.2 Possible Extensions to Moving Probes

When the probe is in motion with respect to the plasma the problem of determining the ambient plasma density in terms of the collected current becomes even more difficult. If the motion is supersonic a detached shock will precede the (spherical) probe; outside the shock the flow will be uniform, and inside the shock there will be a region of

incompressible flow. Qualitatively, one can say that significant electrical effects on the charged particles will be restricted to the sheath surrounding the probe. For high probe potentials and a weakly ionized gas the sheath may extend well beyond the shock. Quantitatively, the problem would be very difficult. Also, any ionization caused by the shock would vitiate the theory.

For a subsonic flow a precise mathematical formulation of the problem should be feasible. With laminar flow everywhere around the probe there would be an analytic solution for the flow lines, and in a weakly ionized gas the ionization will not affect the flow of neutral gas. The velocities of the accelerated particles would just be the vector sum of the gas flow velocity and the drift velocity in the electric field. The problem would be two-dimensional with the radial distance and the flow aspect angle the independent variables. Despite being considerably more complicated than the case of a stationary probe, it is felt that solutions can be found to provide a comparison with the results for the stationary probe and an evaluation of the effects of the motion.

APPENDIX A

Choice of the Starting Values for the Numerical Integration

The Poincaré-Lighthill-Kuo method (Tsien, 1956) was used to find compatible starting values for $\bar{x}$, $\phi(\bar{x})$, and $n_+(\bar{x})$ in the numerical integration of Equations (4.7) and (4.8). In the PLK method the dependent variables and the independent variables are expanded in power series of a small parameter of the problem in terms of a parametric variable, in the neighborhood of a singular point. By choosing an appropriate parameterization it is often possible to find an expansion uniformly valid in the region of interest, or in some cases, it is possible to eliminate the singularity altogether (Tsien, 1956).

Equations (4.7) and (4.8) are re-written here for convenience:

$$\bar{x}^4 \frac{d^2\phi}{d\bar{x}^2} = C[n_+ - \exp(-\phi)]/4 \tag{4.7}$$

$$\frac{dn_+}{d\bar{x}} = n_+\frac{d\phi}{d\bar{x}} - 2 \tag{4.8}$$

At $\bar{x} = 0$ the quasi-neutral solution, $n_+ = n_- = e^{-\phi}$, and the boundary condition,

$$\phi(0) = 0 \tag{A.1}$$

substituted into (4.8) imply that $\frac{d\phi}{d\bar{x}} = 1$ at $\bar{x} = 0$. However, $\bar{x} = 0$ is a singular point of (4.7). Therefore, a small, but non-zero value of $\bar{x}$ had to be taken as the starting point for the integration, and a correction term to the expressions for $n_+(\bar{x})$, $\phi(\bar{x})$, and $\frac{d\phi}{d\bar{x}}$ in the quasi-neutral region was necessary.

The PLK method was applied as follows. The small parameter of the problem, ε, was identified as (4/C). Then $\bar{x}$, ϕ, and n_+ were expanded in powers of ε, as functions of the parametric variable η, that is,

$$\bar{x}(\eta) = \eta + \varepsilon\bar{x}_1(\eta) + \varepsilon^2\bar{x}_2(\eta) + \ldots \qquad (A.2)$$

$$\phi(\eta) = \phi_0(\eta) + \varepsilon\phi_1(\eta) + \varepsilon^2\phi_2(\eta) + \ldots \qquad (A.3)$$

$$n_+(\eta) = n_{+0}(\eta) + \varepsilon n_{+1}(\eta) + \varepsilon^2 n_{+2}(\eta) + \ldots \qquad (A.4)$$

The derivative of the potential, $\frac{d\phi}{d\bar{x}}$, was not expanded since its starting value was to be found by an iterative routine in the computer program (see Appendix B).

Before carrying out the expansions (A.2), (A.3), and (A.4) it was necessary to derive the converted boundary condition on $\phi(\eta)$ at $\eta = 0$, corresponding to $\phi(\bar{x}) = 0$ at $\bar{x} = 0$. This derivation is now presented. At $\bar{x} = 0$ (A.2) becomes

$$0 = \eta_0 + \varepsilon\bar{x}_1(\eta_0) + \varepsilon^2\bar{x}_2(\eta_0) + \ldots \qquad (A.5)$$

where η_0 is the η-coordinate corresponding to $\bar{x} = 0$. Solving (A.5) for η_0 and then inserting the result into the arguments of $\bar{x}_1$ and $\bar{x}_2$ in (A.5) yields

$$\eta_0 = -\varepsilon\bar{x}_1(-\varepsilon\bar{x}_1(\eta_0) - \varepsilon^2\bar{x}_2(\eta_0) + \ldots) - \varepsilon^2\bar{x}_2(-\varepsilon\bar{x}_1(\eta_0) - \varepsilon^2\bar{x}_2(\eta_0) - \ldots). \qquad (A.6)$$

Dropping terms of the order of ε^2 in (A.6), and noticing that

$$\frac{\bar{x}_1(-\varepsilon\bar{x}_1(\eta_0)) - \bar{x}_1(0)}{-\varepsilon\bar{x}_1(\eta_0)} \approx \left(\frac{d\bar{x}_1}{d\eta}\right)_{\eta=0}$$

for $\varepsilon\bar{x}_1(\eta_0) \ll 1$, it is found from (A.6), to first order in ε,

$$\eta_0 = -\varepsilon\bar{x}_1(0) \quad . \tag{A.7}$$

Now at $\bar{x} = 0$, or $\eta = \eta_0$, (A.3) becomes

$$0 = \phi_0(\eta_0) + \varepsilon\phi_1(\eta_0) + \ldots \tag{A.8}$$

where η_0 is given by (A.7). Then by noticing that

$$\frac{\phi_0(-\varepsilon\bar{x}_1(0) - \phi_0(0)}{-\varepsilon\bar{x}_1(0)} \approx \left(\frac{d\phi_0}{d\eta}\right)_{\eta=0} \quad , \tag{A.9}$$

again for $\varepsilon\bar{x}_1(0) \ll 1$, the following relation is obtained after dropping terms of order ε^2

$$0 = \phi_0(0) - \varepsilon\left(\bar{x}\,\frac{d\phi_1}{d\eta}\right)_{\eta=0} = \varepsilon\phi_1(0) \quad . \tag{A.10}$$

Equating coefficients of the ε^0 and ε terms yields

$$\phi_0(0) = 0 \tag{A.11}$$

and

$$\phi_1(0) = \bar{x}_1(0) \left(\frac{d\phi_0}{d\eta}\right)_{\eta=0} \tag{A.12}$$

Before proceeding to expand the variables according to (A.2), (A.3), and (A.4) it is necessary to write down the expression for the operator, $\frac{d}{d\bar{x}}$. Since $\frac{d}{d\bar{x}} = \frac{d\eta}{d\bar{x}} \frac{d}{d\bar{\eta}}$, an approximate form of the operator, exact through first order in ε, is

$$\frac{d}{d\bar{x}} = \left[1 - \varepsilon \frac{d\bar{x}_1}{d\eta}\right] \frac{d}{d\eta} \quad , \tag{A.13}$$

which is obtained by solving (A.2) for η and forming $\frac{d\eta}{d\bar{x}}$. Also it should be noticed that

$$\exp(-\phi) = \exp(-\phi_0) \exp(-\varepsilon\phi_1) \ldots \approx \exp(-\phi_0) [1 - \varepsilon\phi_1] \quad , \tag{A.14}$$

and

$$\bar{x}^4 = \eta^4 + 4\varepsilon\eta^3 \bar{x}_1(\eta) \tag{A.15}$$

through first order in ε.

By immediately dropping terms of order ε^2, Equation (4.7) becomes

$$\varepsilon(\eta^4 + 4\varepsilon\eta^3 \bar{x}_1) \left(1 - \varepsilon \frac{d\bar{x}_1}{d\eta}\right)\left[\left(1 - \varepsilon \frac{d\bar{x}_1}{d\eta}\right)\left(\frac{d^2\phi_0}{d\eta^2} + \varepsilon \frac{d^2\phi_1}{d\eta^2}\right)\right.$$

$$\left. - \varepsilon \frac{d^2\bar{x}_1}{d\eta^2} \left(\frac{d\phi_0}{d\eta} + \varepsilon \frac{d\phi_1}{d\eta}\right)\right] = [n_{+0} + \varepsilon n_{+1} - \exp(-\phi_0) (1 - \varepsilon\phi_1)] \tag{A.16}$$

Equation (4.8) becomes

$$\left(1 - \varepsilon \frac{d\bar{x}_1}{d\eta}\right)\left(\frac{dn_{+0}}{d\eta} + \varepsilon \frac{dn_{+1}}{d\eta}\right) = \left(1 - \varepsilon \frac{d\bar{x}_1}{d\eta}\right)\left(\frac{d\phi_0}{d\eta} + \varepsilon \frac{d\phi_1}{d\eta}\right)(n_{+0} + \varepsilon n_{+1}) - 2 \quad (A.17)$$

Equating coefficients of the ε^0 terms on both sides of (A.16) leads to

$$n_{+0} = \exp(-\phi_0) \quad . \quad (A.18)$$

Similarly from (A.17) one obtains

$$\exp(-\phi_0) \quad \frac{d\phi_0}{d\eta} = 1 \quad (A.19)$$

By employing the boundary condition, (A.11), one obtains

$$n_{+0} = 1 - \eta \quad (A.20)$$

and

$$\phi_0 = -\ln(1 - \eta) \quad (A.21)$$

as the solutions of (A.18) and (A.19).

Equating the coefficients of ε on both sides of (A.16) and using (A.21) leads to

$$\eta^4/(1-\eta)^2 = n_{+1} + (1-\eta)\phi_1 \quad . \quad (A.22)$$

Similarly from (A.17) one derives

$$2\frac{d\bar{x}_1}{d\eta} = n_{+1}/(1-\eta) - \frac{dn_{+1}}{d\eta} + (1-\eta)\frac{d\phi_1}{d\eta} . \qquad (A.23)$$

Combining (A.22) and (A.23) one obtains

$$2\frac{d\bar{x}_1}{d\eta} = \eta^4/(1-\eta)^3 - \frac{d}{d\eta}[\eta^4/(1-\eta)^2] - 2\eta\frac{d\phi_1}{d\eta} - 2\phi_1 \qquad (A.24)$$

Now the freedom in the choice of parameterization allows one to set

$$2\eta\frac{d\phi_1}{d\eta} + \phi_1 = 0 \qquad (A.25)$$

to simplify the differential equation, (A.24), for $\bar{x}_1(\eta)$. Equation (A.25) has the solution $\phi_1 = Y\eta^{-1/2}$, where Y is an arbitrary constant. Since the potential is bounded, Y must be zero. Equation (A.24) can then be integrated after a partial-fraction expansion. After applying the boundary condition, (A.12), for $\bar{x}_1(0)$ one obtains

$$\bar{x}_1 = -[(\eta+7)(\eta-1) + 12\ln(1-\eta) + 8/(1-\eta) - 1/(1-\eta)^2 + 2\eta^4/(1-\eta)^2]/4 \qquad (A.26)$$

From (A.22) one obtains $n_{+1} = \eta^4/(1-\eta)^2$ since $\phi_1 = 0$.

Summarizing, the expressions for $\bar{x}$, n_+, and ϕ through first order in ε are

$$\bar{x} = \eta - [(\eta+7)(\eta-1) + 12\ln(1-\eta) + 8/(1-\eta) - 1/(1-\eta)^2 + 2\eta^4/(1-\eta)^2]/C \qquad (A.27)$$

$$n_+ = (1-\eta) + (4/C)\eta^4/(1-\eta)^2 \qquad (A.28)$$

$$\phi = -\ln(1-\eta) \qquad (A.29)$$

where (4/C) has been substituted back for ε.

The expressions (A.27), (A.28), and (A.29) were used to find the appropriate starting values for the numerical integration of (4.7) and (4.8). For each numerical integration a value of the parameter, C, and a value of the parametric variable, η, were given to the computer as input data (see Appendix B). Typically, η was 0.3 or 0.4. The results of the numerical integrations were checked for sensitivity to starting values by changing the value of η by 0.1 or 0.2 and repeating the integration (see Section 5.1).

Equation (5.1) was also solved by numerical integration (see Section 5.1). The starting values of $\bar{x}$ and ϕ, as obtained by PLK technique, are

$$\bar{x} = \eta + [1/(1-\eta)^2 - 8/(1-\eta) - 12\ \ln(1-\eta) + 8(1-\eta) - 1/(1-\eta)^2]/C \qquad (A.30)$$

and

$$\phi = -\ln(1-\eta) \qquad (A.31)$$

It should be noted that (A.30) disagrees with that obtained by Su and Lam (1963). Equation (A.30) is correct, however, as was confirmed by Su (1966). The starting value for $\frac{d\phi}{d\bar{x}}$ was also obtained by the PLK method when Equation (5.1) was solved. The expression used in the numerical integrations was

$$\frac{d\phi}{d\bar{x}} = 1/(1-\eta) - 2[1 - 4/(1-\eta) + 6/(1-\eta)^2 - 4/(1-\eta)^3 + 1/(1-\eta)^4]/C \qquad (A.32)$$

APPENDIX B

The Computer Program

The numerical integrations were performed by the Illiac II computer of the Department of Computer Science, University of Illinois. In the computer program the physical variables took the following names:

$\bar{x} \rightarrow x$

$n_+ \rightarrow Y(1)$

$\phi \rightarrow Y(2)$

$\frac{d\phi}{d\bar{x}} \rightarrow Y(3)$

$n_- \rightarrow YFOUR$

The numerical integration was executed by a Runge-Kutta-Gill routine (Gill, 1951) which appears in the section of the program written in the NICAP language. NICAP is the machine language of Illiac II.

Equations (4.7) and (4.8) appear between statement 100 and statement 60 of the program. The correct starting value was found by the iterative loop which begins at statement 49.

When Equation (5.1) was integrated the starting value for Y(3) was found by the PLK method and the expression (A.31) from Appendix A was used in place of the iterative loop.

The computer program follows.

```
 47023CICERONE RALPH J  C          003 003  0025  0000EE
$       FORTRAN
$       PUNCH OBJECT
$       GO
       DIMENSION Y(4), DY(4), STR(4)
  800 RIT 7, 801, ETA, C, STRTHI, STRTLW, XPRNT
  801 FORMAT (5F15.0)
       WOT 6, 600, C
  600 FORMAT(1H1//10X13H THE CASE C =, F9.3, 1H.//)
       STARTX = 0.0
       Z = 0.0
       JAM = 0
       JIG = 0
C      THE STARTING VALUE FOR Y(3) IS FOUND BY ITERATION
   49 START = (STRTHI + STRTLW)/2.0
C      THE STARTING VALUE IS CHECKED TO DETERMINE IF IT HAS BEEN
C      CALCULATED TO  MACHINE ACCURACY
       IF (STARTX - START) 500, 501, 500
  500 WOT 6, 404, START
  404 FORMAT(1H0//10X49H THE STARTING VALUE FOR Y(3) IN THIS SEQUENCE IS
      1 , 1PE20.12, 1H./)
       STARTX = START
C      THE STARTING VALUES FOR THE INTEGRATION ARE GIVEN BY THE PLK
C      CORRECTION TO THE QUASI-NEUTRAL SOLUTION
   55 X = ETA -((ETA+7.0)*(ETA-1.0) +12.0*ELOG(1.0-ETA) +8.0/(1.0-ETA)
      1 -1.0/((1.0-ETA)**2) +(2.0*ETA**4)/((1.0-ETA)**2))/C
       Y(1) = 1.0 -ETA + (4.0*ETA**4)/(C*(1.0-ETA)**2)
       Y(2) = -FLOG(1.0-ETA)
       Y(3) = START
       DELTAX = 0.01
       YONE = Y(1)
       YTHREE = Y(3)
   50 YFOUR = EXP(-Y(2))
C       THE PRINTING IS CONTROLLED
       IF(X-XPRNT) 79, 77, 77
   77 JAZZ = (JAM-JIG*5)
       JAM = JAM + 1
       IF(JAZZ) 79, 78, 78
   78 WOT 6, 403, (Y(I), I = 1,3), YFOUR, X
  403 FORMAT(10X7H Y(1) =, 1PE15.8, 11H     Y(2) =, 1PE15.8, 11H     Y(3
      1) =, 1PE15.8, 11H     Y(4) =, 1PE15.8, 8H     X =, 1PE12.5)
       JIG = JIG + 1
   79 IF(YONE - Y(1)) 80, 81, 81
C      THE ION DENSITY MUST BE MONOTONICALLY DECREASING, THE STARTING
C      VALUE FOR Y(3) IS TOO BIG.
   80 STRTHI = START
       GO TO 300
   81 IF(Y(1)*Y(3)) 82, 82, 29
C      THE ION DENSITY AND Y(3) MUST BE POSITIVE, THE STARTING VALUE FOR
C      Y(3) IS TOO SMALL.
   82 STRTLW = START
       GO TO 300
   29 YONE = Y(1)
C      THE SOLUTION SIMPLIFIES WHEN Y(3) APPROACHES AN ASYMPTOTIC VALUE
C      THE INTEGRATION IS TERMINATED IF THE AYMPTOTIC VALUE IS ATTAINED
       IF((Y(3) - YTHREE) -0.0000001) 270, 270, 30
  270 IF(X-2.0) 30, 30, 70
   70 IF(Z) 503, 71, 503
   71 WOT 6, 72, Y(3)
   72 FORMAT(1H0//10X32H THE ASYMPTOTIC VALUE OF Y(3) IS , 1PE15.8, 1H.//
      1)
```

```
      Z = 1.0
      XPRNT = 0.0
      GO TO 55
   30 YTHREE = Y(3)
      CALL SETRKD(4, Y, DY, STR, X, DELTAX)
      Y(4) = X
   51 I = RKDEQ(0)
      GO TO (100, 200), I
  100 X = Y(4)
      DY(1) = Y(1)*Y(3) -2.0
      DY(2) = Y(3)
      IF(Y(2) -20.0) 60, 60, 61
   60 DY(3) = C*(Y(1) -EXP(-Y(2)))/(4.0*X**4)
      DY(4) = 1
      GO TO 51
   61 DY(3) = C*Y(1)/(4.0*X**4)
      DY(4) = 1
      GO TO 51
  200 X = Y(4)
      IF(X-1000.0) 50, 50, 80
  300 YFOUR = EXP(-Y(2))
      WOT 6, 403, (Y(I), I = 1,3), YFOUR, X
      GO TO 49
  501 IF(Z) 503, 502, 503
  502 WOT 6, 406, START
  406 FORMAT(1H0/10X82H THE STARTING VALUE FOR Y(3) HAS BEEN DETERMINED
     1TO MACHINE ACCURACY. THE VALUE IS, 1PE20.12, 1H.//)
      XPRNT = 0.0
      Z = 1.0
      YTHREE = 0.0
      GO TO 55
  503 GO TO 800
      END
```

```
$       NICAP
$       PUNCH OBJECT
        ENTRY  RKDFQ,SETRKD
SETRKD  SFR    5,T
        SFR    6,T+1
        SFR    7,T+2
        LFR    5,COUNTS
        ATN    3,1,
        LFR    F6
        CAD    M8
        SIA    M8
        CSM    MINUSN,M8
        SFR    6,POINTR
        SFR    6,S+1
        ATN    3,1,
        LFR    F7
        CAM    13,STEPSZ
        CAM    H,M13
        SFR    5,COUNTS
        SFR    5,S
        LFR    5,T
        LFR    6,T+1
        LFR    7,T+2
        JLH    M3
RKG2    SFR    5,S
        SFR    6,S+1
RKG6    LFR    4,T
        LFR    5,T+1
        LFR    6,T+2
        LFR    7,T+3
        CAD    1.
        JLH    M3+1
RKDFQ   SFR    4,T
        SFR    5,T+1
        SFR    6,T+2
        SFR    7,T+3
        LFR    7,TOGGLE
        JNM    12,RKD2
RKD1    LFR    5,S
        LFR    6,POINTR
        LFR    2,H
        FLD
        CAD    KSTR
        MPY    F2
        STR    KSTR,1,
        CJF    MINUSN
        LFR    6,S+1
RKG3    CSB    TSTR
        MPY    CONSTS,1,
        ADD    KSTR
        MPY    CONSTS
        STR    F2
        ASC    YSTR,1,
        CAD    F2
        MPY    3.
        STR    F2
        CSB    KSTR,1,
        ADN    COUNT1,1
        CAM    TEST
        MPY    CONSTS,1,
        JNM    TEST,RKG4
```

```
        MPY     3.
RKG4    ADD     F2
        ASC     TSTR,1,
        CJZ     MINUSN,RKG5
        ADM     CONSTS,-2
        TRA     RKG3
RKG5    LFR     6,POINTR
        CJU     COUNT1,RKG7
        LFR     5,COUNTS
        SFR     5,S
        LFR     6,POINTR
        SFR     6,S+1
        CNM     M12
        SFR     7,TOGGLE
        CAD     2.
        LFR     4,T
        LFR     5,T+1
        LFR     6,T+2
        LFR     7,T+3
        JLH     M3+1
RKD2    LFR     7,BLANKS
        SFR     7,TOGGLE
        LFR     6,POINTR
        FLD
        ATN     TSTR,1,
        SFR     F7
        CJF     MINUSN
        TRA     RKG6
BLANKS  BSS     1
S       BSS     2
T       BSS     4
TOGGLE  DECQL   -1,,,
POINTR  DECQL   ,,,
COUNTS  DECQL   RKGC,0,-4,0
RKGC    OCTQ    4000,,,1,4000,,,
        OCTQ    2000,,,1,453,16606,6300,6201
        OCTQ    2000,,,1
        OCTQ    3324,1171,11477,11601,4000,,,1
        OCTQ    5252,12525,5252,12577
STEPSZ  DEC     .010
TEST    EQUM    M3
CONSTS  EQUM    M4
H       EQUM    M5
COUNT1  EQUM    M6
N       EQUM    M7
MINUSN  EQUM    M8
YSTR    EQUM    M9
KSTR    EQUM    M10
TSTR    EQUM    M11
        GO
```

REFERENCES

Appleton, E. V., and J. A. Ratcliffe (1930), Some simultaneous observations on down-coming wireless waves, Proc. Roy. Soc. A128, 133-158.

Balmain, K. G. (1966), Plasma probe studies, Aeronomy Report No. 11, University of Illinois, Urbana, Illinois.

Belrose, J. S. (1965), The lower ionospheric regions, Physics of the Earth's Upper Atmosphere, eds. C. O. Hines, et al., Prentice-Hall, Englewood Cliffs, New Jersey, 46.

Belrose, J. S., and M. J. Burke (1964), Study of the lower ionosphere using partial reflection. Part I. Experimental technique and methods of analysis, J. Geophys. Res. 69, 2799-2818.

Bettinger, R. T., and E. H. Walker (1964), University of Maryland Physics Department Technical Report No. 350 (see also Phyiscs of Fluids 8, 748-751, 1965).

Boggess, R. L. (1959), Electrostatic probe measurements of the ionosphere, Scientific Report No. GS-1, Space Physics Research Laboratory, University of Michigan, Ann Arbor, Michigan.

Bourdeau, R. E., E. C. Whipple, and J. F. Clark (1959), Analytic and experimental electrical conductivity between the stratosphere and ionosphere, J. Geophys. Res. 64, 1363-1370.

Bowhill, S. A., and E. R. Schmerling (1961), The distribution of electrons in the ionosphere, Advances in Electronics and Electron Physics 15, 265-326.

Boyd, R. L. F. (1951), The mechanism of positive ion collection by a spherical probe in a dense gas, Proc. Phys. Soc. of London, B64, 795-804.

Boyd, R. L. F. (1965), Direct measurement techniques for ionization density in the high collision regime, Aeronomy Report No. 10, eds. Sechrist, C. F. and J. S. Shirke, University of Illinois, Urbana, Illinois, 37-40.

Boyd, R. L. F. (1966), Private communication (to be published).

Chalmers, J. Alan (1957), Atmospheric Electricity, Pergamon Press, London, 128.

Champion, K. S. W., and R. A. Minzer (1963), Revision of U. S. Standard Atmosphere 90 to 700 km, Revs. of Geophys. 1, 57-84.

Chen, F. F. (1965), Electric probes, in Plasma Diagnostic Techniques, ed. R. H. Huddlestone, et al., Academic Press, New York, N. Y., 113-200.

Cohen, Ira M. (1963), Princeton University Plasma Physics Laboratory Matt-180, Princeton, New Jersey (see also Physics of Fluids 6, 1492-1499).

Gill, S. (1951), A process for the step-by-step integration of differential equations in an automatic digital computing machine, Proc. Cambridge Phil. Soc. 47, 96-108.

Hoult, D. P. (1965), D-region probe theory, J. Geophys. Res. 70, 3183-3187.

Jackson, J. D. (1963), Classical Electrodynamics, John Wiley and Sons, Inc., New York, 342.

Krasnushkin, P. Y., and N. L. Kolesnikov (1962), Investigation of the lower ionosphere by means of long radio waves and low frequency probes installed on a rocket. Detection of a new ionospheric layer, Akad. Nauk Doklady (USSR) 146, 596.

McDaniel, E. W. (1964), Collision Phenomena in Ionized Gases, John Wiley and Sons, New York, N. Y., Chapters 8 and 9.

Mott-Smith, H. M., and I. Langmuir (1926), The theory of collectors in gaseous discharges, Phys. Rev. 28, 727-763.

Nicolet, M., and A. C. Aikin (1960), The formation of the D-region of the ionosphere, J. Geophys. Res. 65, 1469-1483.

Sagalyn, R. C., and M. Smiddy (1964), Rocket investigations of the electrical structure of the lower ionosphere, Space Research IV, North-Holland Publishing Co., Amsterdam.

Sagalyn, R. C. (1965), The theory of ion collection in the ionospheric D-region, Aeronomy Report No. 10, eds. Sechrist, C. F., and J. S. Shirke, University of Illinois, Urbana, Illinois, 41-43.

Salah, J. E., and S. A. Bowhill (1966), Collision frequencies and electron temperatures in the lower ionosphere, Aeronomy Report No. 14, University of Illinois, Urbana, Illinois, 90.

Sena, L. (1946), J. Tech. Phys., USSR 28, 715.

Smith, L. G. (1965), Langmuir probes for measurements in the ionosphere, GCA Technical Report No. 65-25-N.

Smith, L. G., L. H. Weeks, and P. J. McKinnon (1965), Investigation of the D- and E-regions of the ionosphere during IQSY, GCA Technical Report No. 65-21-N.

Spencer, N. W., L. H. Brace, G. R. Curignon, D. R. Taeusch, and H. Niemann (1965), Electron and molecular temperatures and density in the thermosphere, J. Geophys. Res. 70, 2665-2698.

Su, C. H. (1966), Private communication.

Su, C. H., and S. H. Lam (1963), Continuum theory of electrostatic probes, Physics of Fluids 6, 1479-1491.

Su, C. H., and Ain A. Sonin (1967), Theory of the electrostatic probe in a moderately ionized gas, Physics of Fluids 10, 124-126.

Tsien, H. S. (1956), The Poincaré-Lighthill-Kuo method, in Advances in Applied Mechanics IV, Academic Press, New York, 281-349.

Wasserstrom, Eliahu, C. H. Su, and R. F. Probstein (1965), Kinetic theory approach to electrostatic probes, Physics of Fluids 8, 56-72.

Whitten, R. C., and I. G. Poppoff (1965), Physics of the Lower Ionosphere, Prentice-Hall, Englewood Cliffs, New Jersey, 1.